

UNIVERSITÀ
DI PAVIA

Dipartimento di Biologia e Biotecnologie
"Lazzaro Spallanzani"

Laurea Magistralis in Molecular Biology and Genetics

Cellulolytic potential of *Bacillus* strains: a comparative study for the bioactive paper development.

Potenziale cellulosolitico di ceppi di *Bacillus*: uno studio comparativo per lo sviluppo di carta bioattiva

Supervisor:
Prof. Cinzia Calvio

Co-supervisor:
Prof. Giorgio Ulisse Salvatore Scarì

Experimental thesis by
Francesca Sarati

Academic Year 2025/2026

ABSTRACT

The global consumption of Flushable Consumer Products (FCPs), particularly toilet paper, presents significant environmental and infrastructural challenges, representing a primary cause of sewer pipe blockages. Bacterial bioremediation offers a sustainable solution by incorporating bacterial spores into tissue paper to accelerate substrate degradation post-disposal. Among candidate microorganisms, species of the genus *Bacillus* stand out for their robust sporulation capacity, non-pathogenic safety profiles, and powerful extracellular cellulolytic machinery.

This work investigates the cellulolytic potential and biosafety profiles of three wild-type strains (*Bacillus subtilis, Bacillus velezensis,* and *Bacillus amyloliquefaciens*) alongside an engineered non-GMO *Bacillus subtilis* strain (PB5946) to evaluate their suitability for bioactive paper development. Bioinformatic genome screening confirmed the presence of key endoglucanase and β-glucosidase genes while establishing a clean antimicrobial resistance profile across the strains. Phenotypic and kinetic characterizations validated by flow cytometry revealed that the engineered *B. subtilis* PB5946 exhibited superior growth dynamics and cellulase secretion, as demonstrated by enzymatic index assays on carboxymethylcellulose (CMC). Furthermore, scanning electron microscopy and gravimetric mass-loss assays confirmed severe microstructural fiber truncation and significant paper degradation over a seven-day period.

Overall, these approaches highlight how *Bacillus* strains can serve as effective bioactive agents in sustainable tissue paper manufacturing, providing an innovative biotechnological strategy to mitigate sewer infrastructure blockages and contribute to environmentally safe innovations.

RIASSUNTO

Il consumo globale di prodotti monouso lavabili (*Flushable Consumer Products*, FCP), in particolare la carta igienica, presenta significative sfide ambientali e infrastrutturali, rappresentando una delle principali cause di ostruzione delle condutture fognarie. La bioremediazione batterica offre una soluzione sostenibile mediante l'incorporazione di spore batteriche nella carta per accelerare la degradazione del substrato dopo lo smaltimento. Tra i microrganismi candidati, le specie del genere *Bacillus* si distinguono per la loro elevata capacità di sporulazione, i profili di sicurezza non patogeni e un potente apparato cellulosolitico extracellulare.

Questo lavoro analizza il potenziale cellulosolitico e i profili di biosicurezza di tre ceppi wild-type (*Bacillus subtilis*, *Bacillus velezensis* e *Bacillus amyloliquefaciens*) affiancati da un ceppo ingegnerizzato non-GMO di *Bacillus subtilis* (PB5946), al fine di valutarne l'idoneità per lo sviluppo di carta bioattiva. Lo screening bioinformatico del genoma ha confermato la presenza dei geni chiave per endoglucanasi e β-glucosidasi, delineando al contempo un profilo di resistenza agli antibiotici privo di criticità nei diversi ceppi. Le caratterizzazioni fenotipiche e cinetiche validate tramite citometria a flusso hanno rivelato che il ceppo ingegnerizzato *B. subtilis* PB5946 ha mostrato dinamiche di crescita e secrezione di cellulasi superiori, come dimostrato dai saggi dell'indice enzimatico su carbossimetilcellulosa (CMC). Inoltre, la microscopia elettronica a scansione e i saggi gravimetrici di perdita di massa hanno confermato una marcata rottura delle fibre e una significativa degradazione della carta nell'arco di sette giorni.

Nel complesso, questi approcci evidenziano come i ceppi di *Bacillus* possano fungere da efficaci agenti bioattivi nella produzione sostenibile di carta igienica, fornendo un'innovativa strategia biotecnologica per mitigare gli intasamenti delle infrastrutture fognarie e contribuire a innovazioni ecologicamente sicure.

TABLE OF CONTENTS

INTRODUCTION 1

1 Bacillus, a versitile and surprising genus 1

1.1 General characteristics 1

1.2 Industrial applicability of *Bacillus* species 5

1.3 Biosafety profile and regulatory compliance of industrial *Bacillus* strains 6

1.4 Comparison of B. subtilis, B. velezensis and B. amyloliquefaciens 7

2 Cellulase: the paper-eating enzymes 9

3 Bioactive paper as a novel application of bacteria bioremediation 13

3.1 Bioremediation 13

3.2 Toilet paper as the primary flushable pollutant 16

THE AIM OF THE WORK 18

MATHERIALS AND METHODS 19

3.1 Bacillus species and strains 19

3.2 Culture media 19

3.3 Methods used in the study 22

3.3.1 Genome sequencing 22

3.3.2 Bacteria growth 23

3.3.3 Congo Red Assay 25

3.3.4 Scanning Electron Microscopy (SEM) analysis 27

3.3.5 Weight paper lost 29

RESULT AND DISCUSSION 31

4.1 Bioinformatic genomic screening of cellulolytic enzymes and Antimicrobial Resistance (AMR) profiling 31

4.2 Comparative growth kinetics and flow cytometric validation of Bacillus strains 35

4.3 Congo red agar Diffusion Demonstrates Enhanced Cellulase Secretion in Engineered B. subtilis 40

4.4 SEM Analysis Reveals Microstructural Degradation and Fiber Truncation 43

4.5 Gravimetric Weight Loss Analysis of Cellulosic Substrates 47

CONCLUSION 51

REFERENCES 52

Bibliography 52

Sitography 57

INTRODUCTION

1 *Bacillus*, a versatile and surprising genus

1.1 General characteristics

The genus *Bacillus* is one of the most extensively studied genera. Microorganisms belonging to this genus are Gram-positive bacteria that can be aerobic or facultative anaerobic, characterized by endospore formation and broad metabolic plasticity (Alcaraz et al., 2010).

Bacillus genus belongs to the family of Bacillaceae, order of Bacillales, class of Bacilli and phylum of Bacillota (Firmicutes), the same phylum of *Staphylococcus* and *Streptococcus* (Crivelli et al., 2024).

The first description of this genus was provided by Christian Gottfried Ehrenberg, one of the pioneers of microbiology. In 1835, he described what is now known as *Bacillus subtilis* for the first time, naming it *Vibrio subtilis*- presumably owing to its motility (Stülke et al., 2023). Later, the name by which it is known today, *Bacillus subtilis*, was proposed in 1872 by Ferdinand Cohn. Subsequently, the term *Bacillus* was adopted as the name of the entire genus (Harwood, 1989).

For many years this genus was considered a heterogeneus group. However, with the introduction of sequencing technologies and the refinement of taxonomic paramethers 17 distinct clades have been classified within the genus *Bacillus*. Currently, 435 species and 12 subspecies belong to this genus. The most accredited phylogenomic analysis of *Bacillus* genus is by Gupta et al., 2020, where two major distinct clades were proposed: the *subtilis* (*sensu stricto*) clade, in which are grouped all the species used for industrial/agriculture purpose, (such as *B. subtilis, B. velezensis* and *B. amyloliquefaciens*) and the *ceresus* (*sensu lato*) clade, comprising species that caused foodborne illness, anthrax and other illness due to toxins release (Crivelli et al., 2024).

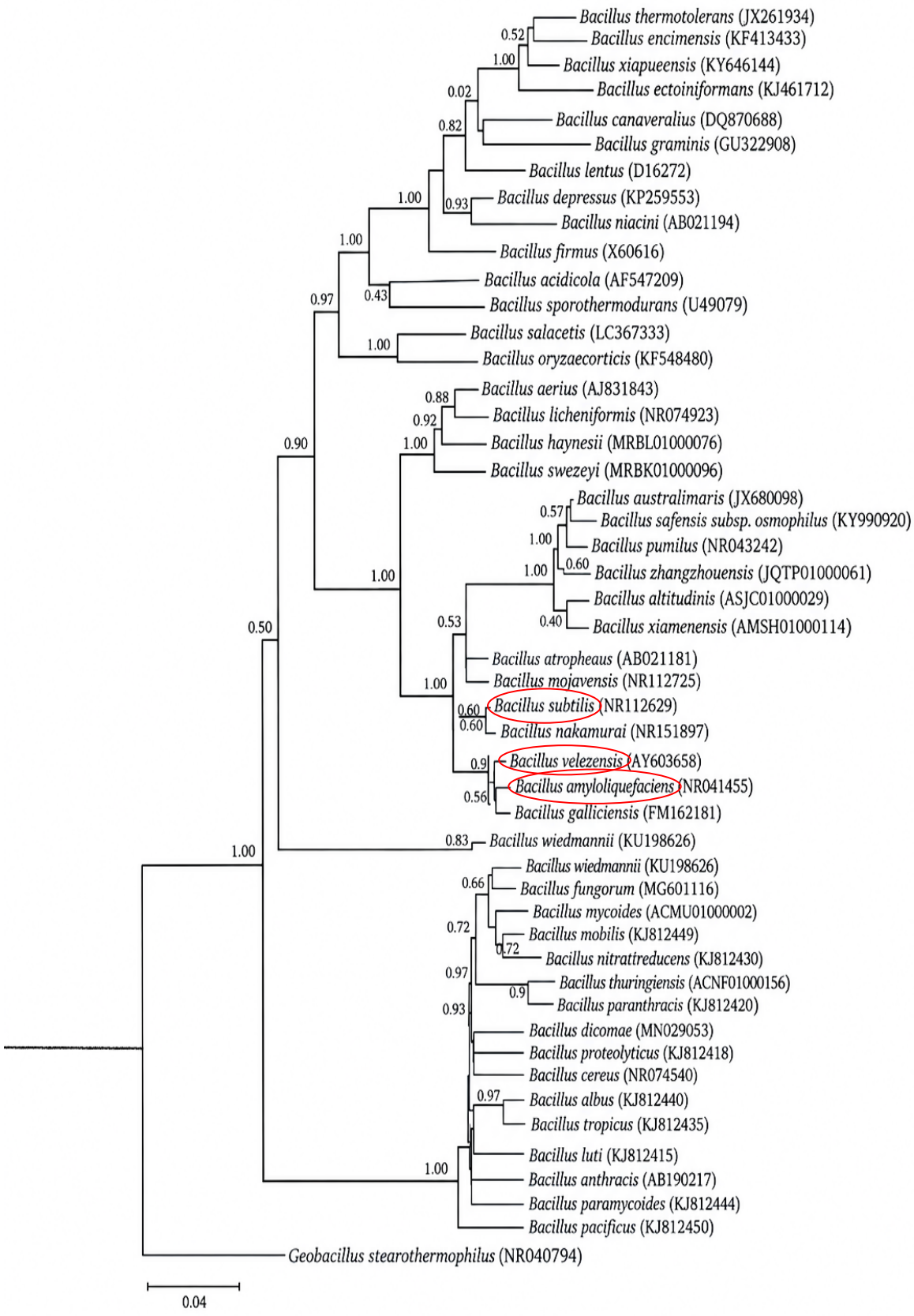


Figure 1.1 Bayesian tree of *Bacillus* genus inferred from 16 S rRNA gene (adapted and modified from Yao et al., 2025). The red circle indicates the species employed for this thesis.

The morphology of *Bacillus* species is characterized by rod-shaped with variable size, between 0,5 and 10 µm. Vegetative cells are typically motile via peritrichous flagella, that cover the entire cell surface (Parra-Cota et al., 2024). These microorganisms have ubiquitous distribution, colonizing terrestrial, aquatic and aerial environments and establishing symbiotic interactions with both plants and animals (Acho-Vasquez et al., 2025).

Bacillus species are characterized by one circular chromosome of approximately 4,2 Mb compacted into a functional non-membrane-bound nucleoid. In some species is also present circular accessory genomes, called plasmid, of 6,9-16 kb, that confers to the bacteria additional characteristics and advantages. The *Bacillus* genome is able to be inherited through Vertical Gene Transfer (VGT) or passed to another organism through Horizontal Gene Transfer (HGT) (Colin, 1989).

In case of vertical gene trasfer, the circular chromosome is replicated following the theta bidiretional model. In this model the replicative fork starts from the origin of replication (*oriC*) in both direction toward the termination site (*terC*). In this way, two identical chromosomes are obtained.

Horizontal gene transfer expands phenotypic diversity in *Bacillus* through natural competence, transduction, and conjugation. These three mechanisms differentiate based on gene vector: in natural competence, free DNA is directly absorbed by the cell; in the transduction the DNA transportation si mediated by a virus while, in conjucation, the DNA trasfer occurs through physical contact between the two cells (Snyder et al., 2020).

Among different features of this genus, one of the most prominent is the capability to transition from a vegetative state to heat-resistant dormant endospore whenever the environment condition becomes adverse. This process is tightly regulated by the master regulator gene *spo0A,* whose transcription is stimulated by high cell density in the environment. Indeed, high cell concentration leads to nutrient deprivation, triggering a cascade of cellular response that prepare the cell to a long period of starvation preventing the cell death.

The sporulation process takes approximately 6-8 hours to be completed and can be divided into 7 different stages. They consist in an asymmetric replication concluding by the embedded of one half to the other one and the mother cell lysis. During these steps both genetic and morphologic change occur.

As soon as the environmental condition become favorable and nutritive molecules are detected a germinative process is undertaken, and the cell returns to vegetative form (Colin, 1989).

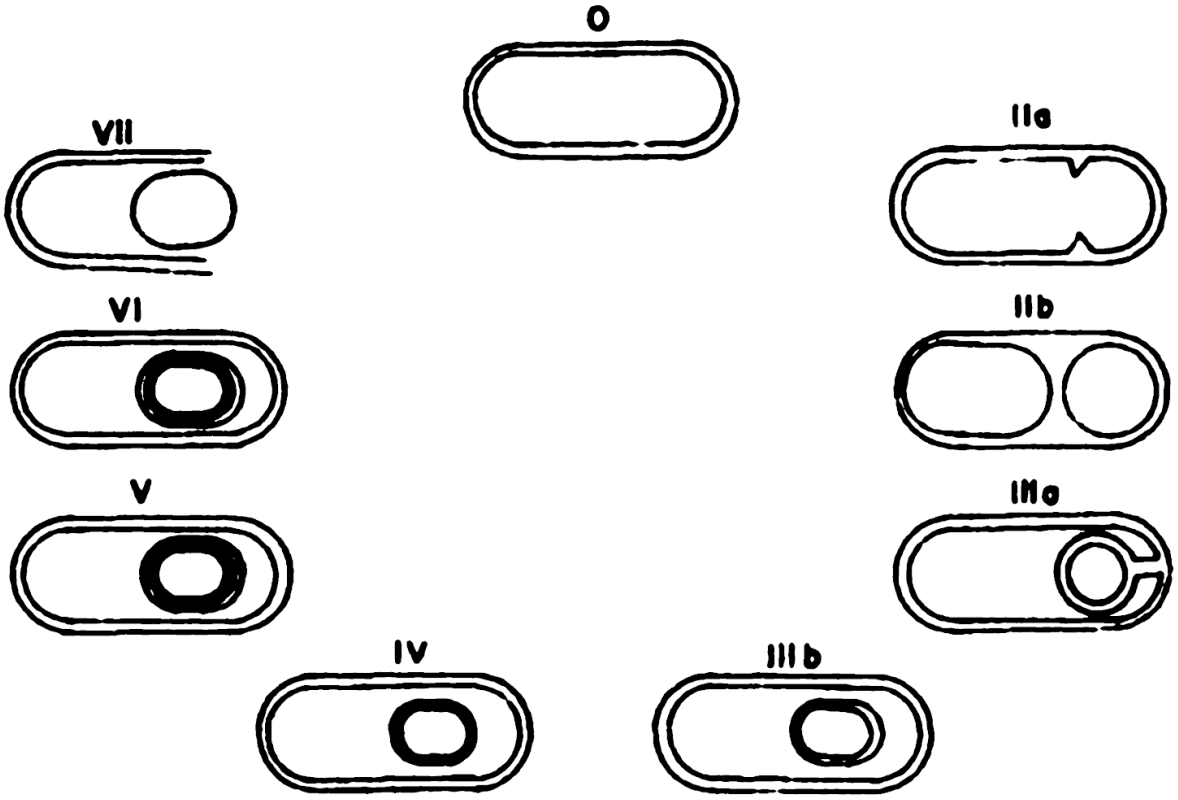


Figure 1.2 Schematic representation of cell morphology modification during the seven steps of sporulation process. From stage 0 to I (initiation) no morphological changes occur but only genetic ones with activation and repression of genes. During stages II and III an asymmetric division takes place, leading to endospore maturation (stages IV-VI) and culminating in mother cell lysis and endospore release (adapted and modified from Colin, 1989).

Biofilm formation is another remarkable characteristic of *Bacillus*. Indeed, rather than functioning as isolated planktonic entities, these bacteria can adopt a sessile, community-based lifestyle. Generally, a biofilm is a structured aggregate of microbial cells enclosed within a self-produced extracellular polymeric substance (EPS) matrix adhering to biotic or abiotic surfaces. Its development is characterized by a dynamic, multi-step process transitioning microbes from free-swimming cells to complex, organized architectures (Erkihun et al., 2024). All the stage that characterizes the biofilm development are directed by another fascinating feature that *Bacillus* possess, quorum sensing. Quorum sensing (QS) is a cell-density-dependent communication mechanism. QS circuits direct

multiple stages of biofilm progression, controlling matrix synthesis and lipopeptide production while also initiating matrix breakdown during the final dispersion phase (Sahreen et al., 2022).
Together, these features (from spore formation to quorum-sensing-regulated biofilms) give *Bacillus* species strong environmental resistance. These characteristics support their widespread use as microbial factories and functional agents across various industrial sectors.

1.2 Industrial applicability of *Bacillus* species

Due to its versatility and ability to produce a wide variety of useful enzymes, interest in the genus *Bacillus* is increasing. As proof of this, in 2020, $18 billion were invested in its market and since 2017, 650 patent were submitted annually, demonstrating the huge market importance.
The applications of *Bacillus* for industrial purposes are extremely varied and encompass food, agriculture, pharmaceuticals, and environmental management (Herrmann et al., 2024).

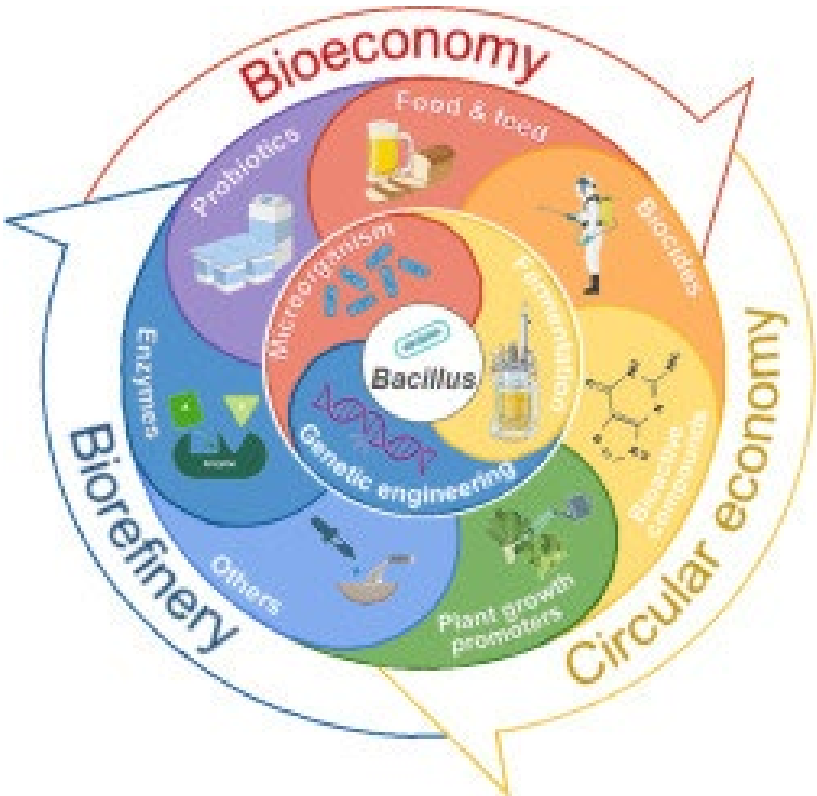


Figure 1.3 Explicative representation of the different fields of application of *Bacillus* species (Herrmann et al., 2024).

In the agricultural sector, for instance, different *Bacillus* species, such as *B. subtilis, B. azotofixans, B. macerans, B. velezensis,* are naturally able to create symbiotic interaction with plant, representing in

this way a biomarker, a protection against diseases, and helps to increase plant defenses against biotic stress (Etesami et al., 2023).

Regarding food industries, *Bacillus* fermentation capacities have been exploited in ancient African and Asian food, such as *natto, miso, tua'nao, kinema, chongkuk-jung, churpi, and dawadawa*.

From a pharmaceutical perspective, owing to their adaptability to diverse environmental conditions, species such as *B. subtilis*, *B. amyloliquefaciens*, and *B. licheniformis* are widely harnessed as probiotics.

These are only a few examples of the industrial applicability of *Bacillus* genus, but the list is remarkably extensive and continues to grow year after year (Herrmann et al., 2024).

1.3 Biosafety profile and regulatory compliance of industrial *Bacillus* strains

The *Bacillus* genus exploitation in industry, as previously mentioned, covered different fields and it is increasing every year. Concerning products intended for human contact, daily-personal care, probiotics, skin care among others, the production must follow stringent rules that certify the microbial safety. In case of the European Union, it does not rely on single legislation and association to classify a bacterium as safe. Across these legal pathways, the European Food Safety Authority (EFSA) conducts scientific risk evaluations, heavily utilizing the Qualified Presumption of Safety (QPS) framework to evaluate non-pathogenic strains (Koutsoumanis et al., 2023). With respect to toilet paper and other dry hygiene items, they fall under the general consumer safety legislation, specifically Directive 2001/95/EC (General Product Safety Directive, updated by Regulation (EU) 2023/988 GPSR). Under this law, manufacturers hold strict legal responsibility for ensuring that the microbiological bioburden on dry goods presents no risk to consumer health (Vincze et al., 2019).

The regulatory landscape is even more complex in the case of Genetically Modified Microbes (GMMs): regulatory agencies impose strict biological safety requirements to prevent systemic spread and ecological contamination (Wegmann et al., 2017). Consequently, relying on non-recombinant optimization strategies offers a clear advantage, fulfilling high safety standards while bypassing cumbersome GMM approval protocols.

Generally, the gold standard to ensure bacteria safeness is to know the precise taxonomy of that species, to establishes identity and rules out related pathogenic lineages, and to verify the lack of toxigenicity and antibiotic resistant (Koutsoumanis et al., 2023). Genomic assessments must verify that resistance profiles are chromosome-borne and non-transferable before an organism is cleared for human use (Wang et al., 2017).

Most *Bacillus* species are considered to be safe for human usage. To be more precise, actually, *Bacillus* contains both extensively utilized probiotic organisms and notable human pathogens. Indeed, following the taxonomic distinction proposed by Gupta et al. (2020), *Bacillus* genus is characterized by two main clades, *subtilis* (*sensu stricto)* and *cereus* (*sensu lato*). While *subtilis*, are considered safe species and broadly industrially applicable, *ceresus* are considered pathogenic members (notably *Bacillus anthracis* and *Bacillus cereus*) able to encode enterotoxins, cytotoxin K, and emetic toxins such as cereulide, which cause foodborne illness and invasive infections (Brutscher et al., 2022). Even if they are considered two different clades, they are strictly related and for these reasons, prior to employing any bacterial strain for industrial purposes, comprehensive bioinformatics analyses regarding virulence and antibiotic resistance are mandatory

1.4 Comparison of *B. subtilis, B. velezensis* and *B. amyloliquefaciens*

The three species selected for this thesis, belonging to the *Bacillus* genus, are characterized by all the incredible features previously described. Indeed, ubiquity, high-temperature resistance, genome plasticity and huge adaptability make these species ideal for industrial purposes.

These three species derived from the same environment, the soil, where they frequently establish symbiotic interactions with plants (Elhameed et al., 2020).

Belonging to the same genus, *B. subtilis, B. velezensis* and *B. amyloliquefaciens* share almost the same morphological characteristics. They are very difficult to distinguish by using classical taxonomic parameters because of morphological and physiological characteristics, cell wall compositions, 16S rRNA sequences and G+C content (Fan et al., 2017). Recent studies, based on the *rpoB* gene, have demonstrated that *B. velezensis* and *B. amyloliquefaciens* are more closely related than *B. subtilis,* belonging to a different subclade with *B. methylotrophicus* and *B. siamensis* (Rabbee et al., 2019).

Among these three species, *B. subtilis* is the best-studied model organism, being a model organism for Gram+, in particular for spore and biofilm characterization, and the first one to be discovered, being the progenitor of the *Bacillus* genus (Stülke et al., 2023).

The discovery of *B. amyloliquefaciens* dates to 1943, by Japanese microbiologist Juichiro Fukumoto, who distinguished it from *Bacillus* subtilis based on its notable ability to produce a liquefying α-amylase. α-amylase is an enzyme that serves as a cornerstone of industrial starch processing, brewing, baking, and textile desizing (Ngalimat et al., 2021)

Chronologically, the last to be discovered was *B. velezensis*: its finding is instead dated in between 1999 and 2000 in the south of Spain (Rabbee et al., 2019). Despite its more recent discovery, *B.*

velezensis has been shown great relevance due to its superior biofilm-forming capacity and higher adaptability (Zeng et al., 2025).

Regardless, all three species are of great industrial interest. Indeed, as with all other *Bacillus* species, *B. subtilis, B. velezensis*, and *B. amyloliquefaciens* are great enzymatic producers. As far as cellulolytic activity is concerned, different studies have tested cellulase production in all three species. For instance, Elhameed et al. (2020) tested and compared the carboxymethyl cellulase activities of five different Bacillus isolates, among them the three species used in this work. The results show that CMCase production was maximal in *B. amyloliquefaciens* compared to *B. subtilis* and *B. velezensis*, but results varied in different process conditions (Elhameed et al., 2020).

2 Cellulase: the paper-eating enzymes

One of the most used and ancient materials is paper: it is composed of different organic polymers, such as lignin, cellulose, hemicellulose and inorganic compounds. Among this cellulose is the most abundant one (Chokshi et al., 2020). Cellulose is a homopolymer of anhydroglucose units linked by β-1,4-glycosidic bonds. In detail, it is made up of a D-glucose unit at the non-reducing end with a C4-OH group, while the terminating group is C1-OH, the reducing end with an aldehyde structure (Figure 2.1)

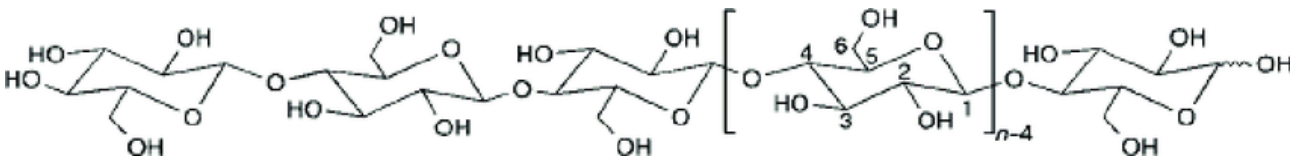


Figure 2.1 Molecular structure of cellulose (Gupta et al., 2019).

Due to its structure (Figure 2.1) it can retain a semi-crystalline state of aggregation even in an aqueous environment, an unusual characteristic for a polysaccharide. This feature, combined with strength and flexibility, makes cellulose extremely interesting in industrial material fields (Gupta et al., 2019).

The natural origin of cellulose makes this polymer fully degradable. Indeed, proteins capable of cleaving this long polymer exist in nature: the cellulase family. These enzymes belong to the class of O-glycoside hydrolases (GH) and are grouped in three categories, endo-β-1,4-glucanases (endoglucanase, EG), exo-β-1,4-glucanases (exoglucanase, CBH) and β-glucosidases (BGL), that act synergistically to reduce this long polymer into glucose monomers (Dobrzyński et al., 2023). The GH proteins are extremely heterogeneous and are divided into 165 families (Liu et al., 2021). More specifically, endoglucanases are grouped in families 5, 6, 7, 8, 12, 44, 45, 48, 51, 64, 71, 74, 81, 87, 124, 128 GH proteins; exoglucanases belong to 5, 6, 7 and 4 GH enzymes, and β-glucosidases in families 1, 3, 4, 17, 30, and 116. Not all the cellulolytic organisms are able to encode all these proteins (Dobrzyński et al., 2023).

The enzymatic reaction is reported in Figure 2.2 underlining the mechanism of action of each cellulase.

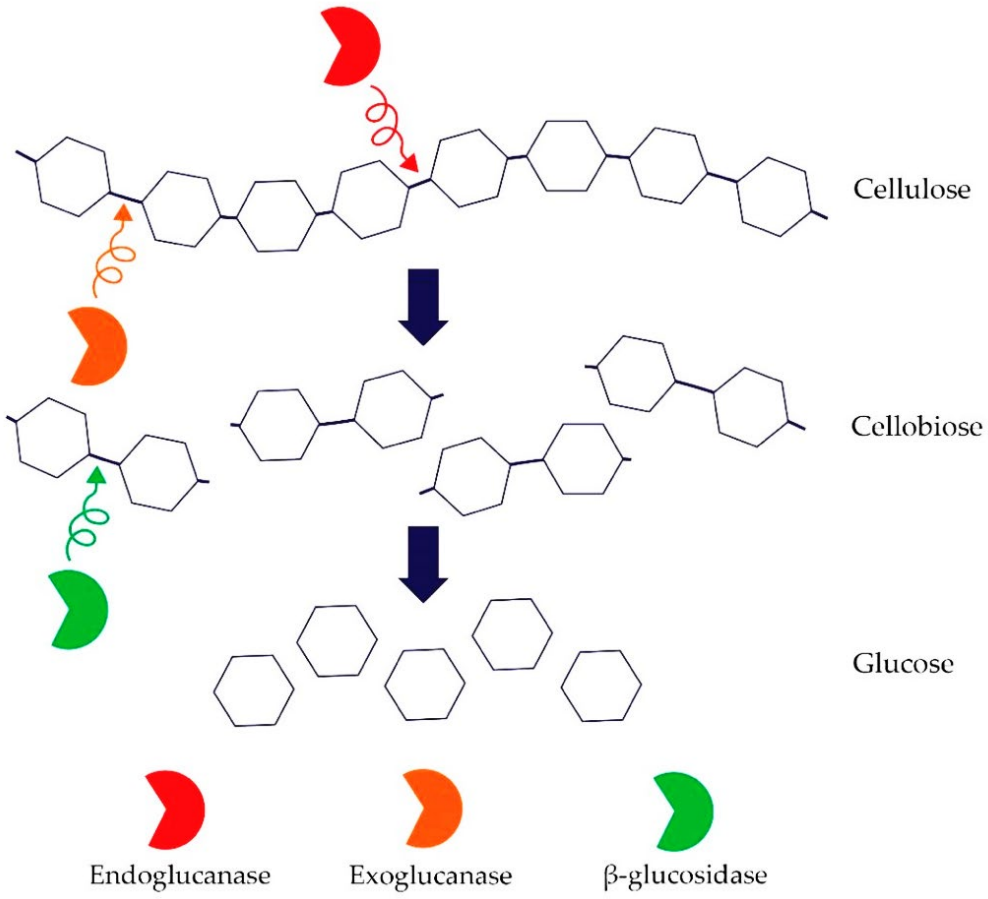


Figure 2.2 Cellulose hydrolysis by the three types of cellulases (Dobrzyński et al., 2023).

Specifically, endo-β-1,4-glucanases catalyze random cleavage of β-1,4-glycosidic bonds in the central part of the polymer. In contrast, exocellulases discard a single glucose molecule from the terminal end of cellulose polymers. By the action of these two enzymes, cellulose is reduced to cellobiose molecules. Indeed, the glucose monomers are obtained by the action of β-glucosidases. The complete degradation of cellulose is achieved only by the synergistic action of all three enzymes (Dobrzyński et al., 2023).

Cellulases can be expressed and secreted by different organisms, such as fungi, actinomycetes and bacteria. Among the cellulolytic bacteria, the most prominent are members of the genus *Bacillus*, showing great relevance in industrial applications (Balla et al., 2022).

The transcriptional expression of cellulase genes in *Bacillus* is tightly regulated. A large number of genes, located on chromosome, are responsible for cellulase transcription. More precisely, cellulase genes in *Bacillus* are co-regulated with genes for sugar transport, peptidoglycan recycling, and protein metabolism through shared operon structures, indicating crosstalk between cellulolytic and other metabolic pathways (Fatani et al., 2021).

The gene expression and location differ based on the species, even when closely related. Moreover, in the case wild-type species belonging to this genus exists that show an incomplete cellulolytic system, usually by lacking exoglucanases production (Liu et al., 2025).

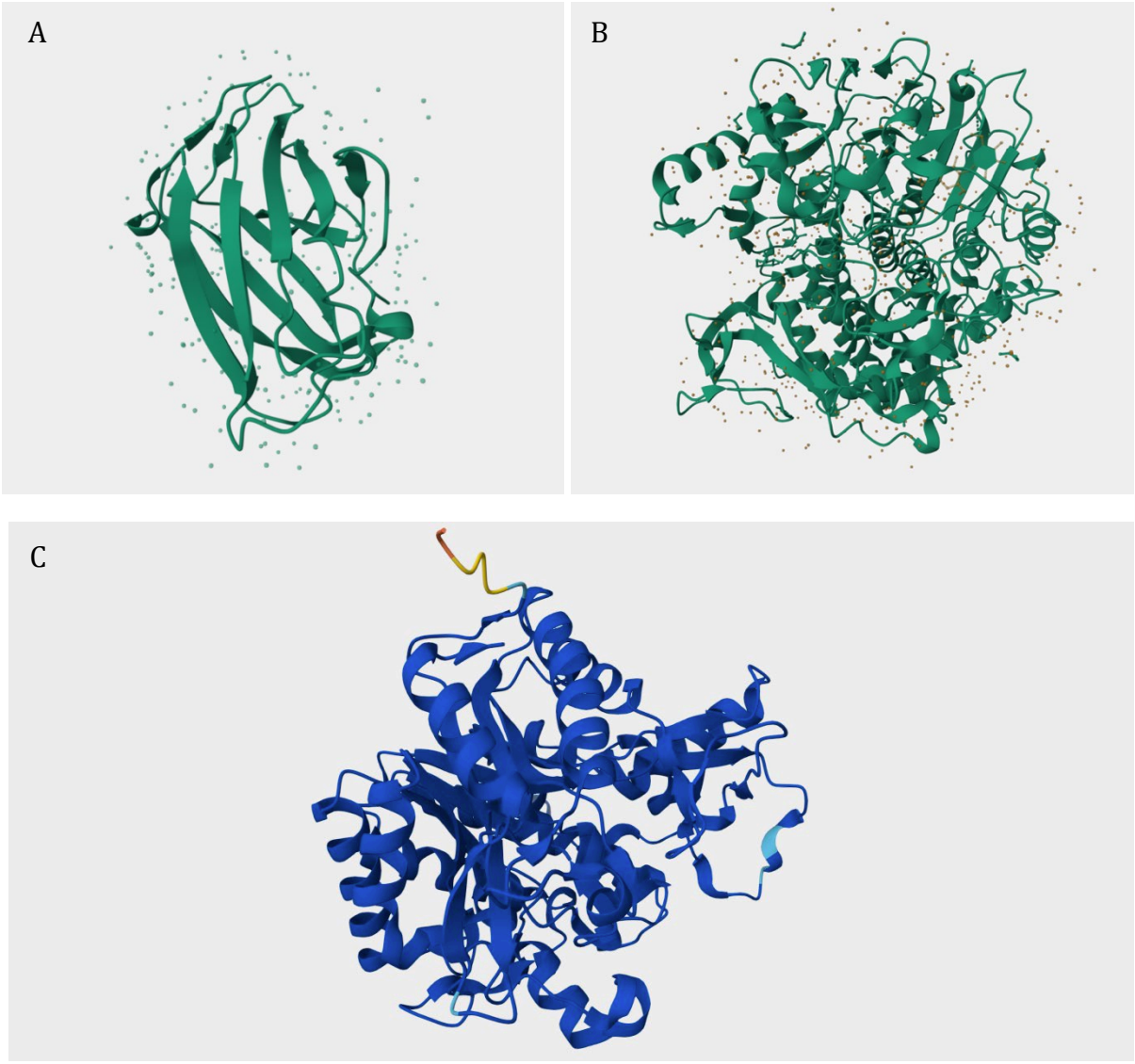


Figure 2.3 Molecular representation of the three cellulases in UniProt database (https://www.uniprot.org); (A) Endo-β-1,4-glucanases (P10475) of *Bacillus subtilis* (strain 168); (B) exo-β-1,4-glucanases (A8FDC4) of *Bacillus pumilus* (strain SAFR-032); (C) β-glucosidases (O05508) of *Bacillus subtilis* (strain 168).

The wide variety of cellulase-encoding genes reflects the enormous diversity in protein structure.
A representative molecular structure of these proteins is shown in Figure 2.3. Generally, cellulases possess a modular architecture comprising a catalytic domain (CD) and a carbohydrate-binding module (CBM, also termed CBD), which are typically interconnected by a flexible, linker region. The catalytic site within the catalytic domain harbors two conserved amino acid residues responsible for glycosidic bond hydrolysis, proceeding via either retention or inversion of the anomeric carbon configuration. Structural divergence across cellulase families is predominantly concentrated at the N- and C-termini, whereas the core catalytic fold remains structurally conserved (Lugani & Sooch, 2017). Over the past few years, the industrial demand for cellulolytic enzymes has increased substantially, expanding their applications across diverse biotechnological sectors.

3 Bioactive paper as a novel application of bacteria bioremediation

3.1 Bioremediation

Over the past century, the industrial field has been growing, giving rise to modern society (Kour et al., 2021; Singh, 2025). The rapid worldwide industrialization together with massive population growth has increased urbanization and intensive agriculture (Singh, 2025). All these factors contribute not only to driving economic growth but have a massive impact on the environment causing different types of pollution compromising essential resources as water, soil and air (Kour et al., 2021).

This is a global issue: more than 12 million tons of hazardous waste materials are produced every year (Singh, 2025). This anthropogenic pressure is caused by both industrialized and developing countries (Dvořák et al., 2017). In the case of the latter, the situation is worse due to a lack of waste treatment infrastructure (Singh, 2025).

The ecologic implication is significant: synthetic compounds released by factories remain in the environment for decades causing long-term ecological impact (Singh, 2025). Extensive literature documents show that the destruction of entire habitat is caused by human contaminants. A stark illustration of environment damage is the marine oil spills leading to catastrophic degradation of its flora and fauna (Matilda & Samuel, 2024).

Pollution has an enormous implication on the ecosystem as well as on public health (Dvořák et al., 2017). A recent report of the World Health Organization, during the World Health Day 2022, reported that one in four global deaths is caused by pollution (World Health Organization, 2022). Prolongated contact with pollutants can cause cancer, reproductive issues, neurological disorders and different types of respiratory diseases such as chronic obstructive pulmonary disease (COPD) and asthma (Ayilara & Babalola, 2023).

Fortunately, human society has been trying to find a solution to this self-inflicted harm. Chemical and physical approaches have been used to reduce the impact of environmental degradation, but they come with their drawbacks, such as high cost of energy, secondary pollution, lack of selectivity and limited applicability (Ayilara & Babalola, 2023; Singh, 2025).

The real paradigm shift in environmental remediation seems to be the bioremediation approach. Bioremediation is a method that takes advantage of the capacity of specific microorganisms (bacteria, fungi or archaea) or plants to convert a pollutant into useful sources of molecules for their metabolism (Ayilara & Babalola, 2023; Singh, 2025). Therefore, this approach closely adheres to the concept of a circular economy, prioritizing environmental restoration through natural, zero-waste biological

processes (Dvořák et al., 2017). Moreover, bioremediation displays particular advantages, including low cost, minimal ecological disturbance, applicability in *in situ* and *ex situ* environments, and the potential for complete mineralization of pollutants (Singh, 2025). For these reasons, bioremediation appears as a promising environmental friendly solution and is highly compatible with the UN Sustainable Development Goals (SDGs), outlined in the 2030 Agenda, particularly SDG 6 (Clean Water and Sanitation), SDG 13 (Climate Action), and SDG 15 (Life on Land) (United Nations, 2015).

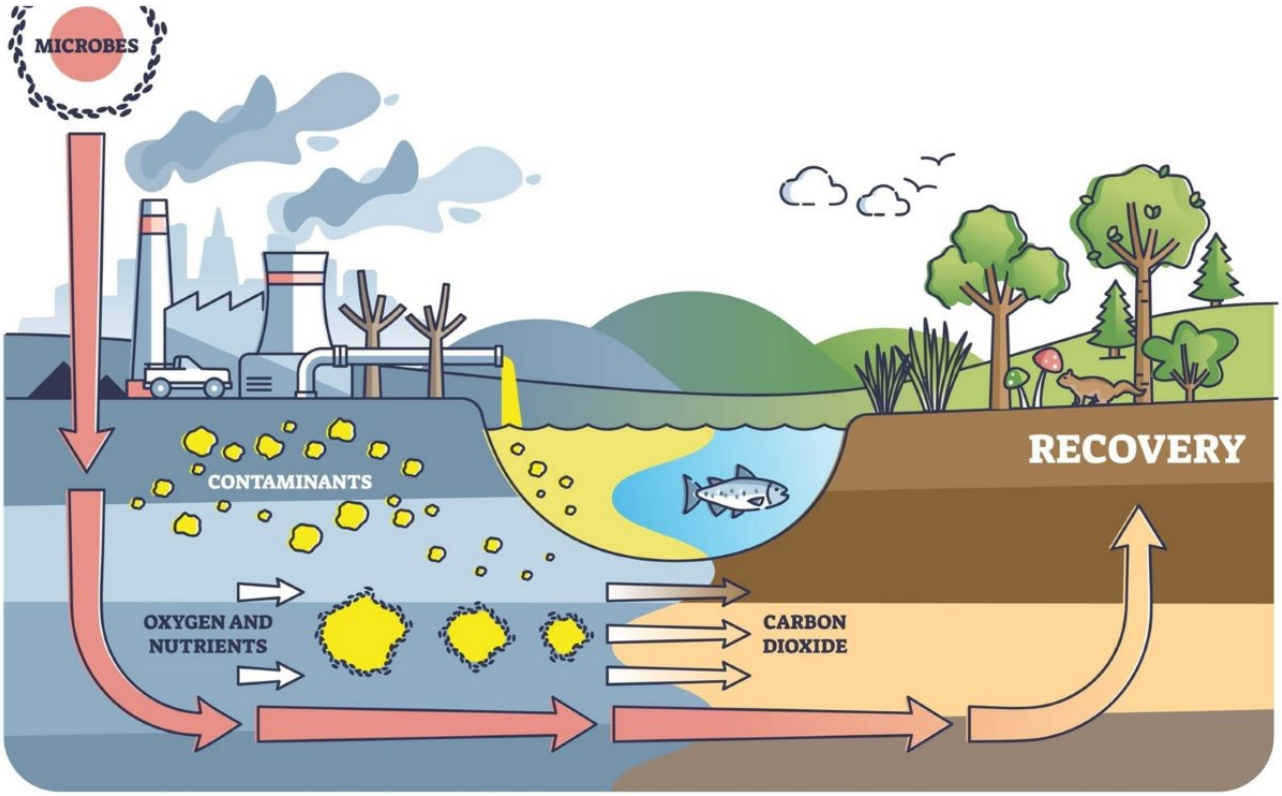


Figure 3.1: Schematic overview of microbial bioremediation, illustrating the enzymatic conversion and detoxification of industrial contaminants into non-toxic metabolic byproducts (Matilda and Samuel, 2024)

Although the concept of bioremediation is relatively recent, first studies on the ability of plants and microorganisms to detoxify pollutant date back to late 19th century with the first attempt of using it as wastewater treatment plant (Dvořák et al., 2017). In the 1970s bioremediation started to increase its scientific value, driven primarily by a seminal paper by Raymond et al., where they demonstrated the capability of indigenous groundwater bacteria to naturally break down petroleum hydrocarbons (Raymond et al., 1975). However, it was only with advancements in bioengineering, coupled with growing concerns over environmental pollution, that bioremediation became formalized as a distinct

scientific field (Singh, 2025). Nowadays, bioremediation is well studied and improves day by day thanks to the emergence of synthetic biology, bioinformatics and all related omics sciences. A robust body of empirical research substantiates data in favors of its success and widespread applicability (Dvořák et al., 2017).

As mentioned previously, bioremediation can be performed by different organisms such as plants, fungi, archaea and bacteria. Among these, bacteria show different advantageous features as rapid proliferation, metabolic versatility, simplicity, rapid evolution, genomic plasticity and the ability of spreading in every habitat (Dvořák et al., 2017; Singh, 2025). In tandem with this, numerous studies have proven that 90-95% of contaminants degrade efficiently if treated with the right bacteria (Singh, 2025).

The metabolic versatility of microorganisms, particularly of bacteria, represents the key determinant in bioremediation. This feature is implementable to treat the major problematic: hydrocarbons, heavy metals and synthetic plastics (Singh, 2025). Although hydrocarbons are not synthetic substances and they consist mainly of carbon and hydrogen, the crude oil processing increases their complexity, toxicity and recalcitrance. Numerous studies have shown that not only there are bacterial community able to live in habitats with hydrocarbons, but also to produce compounds such as biosurfactants, biopolymers, solvents, gases and acids for transforming them bioavailable into carbon and energy sources (Pandolfo et al, 2023). Regarding heavy metals, like arsenic and mercury, the principal difficulty resides in the fact that these pollutants cannot be biodegraded into simpler harmless products. Moreover, their toxicity is important even at low concentration. Encouragingly, different bacteria, as *B. subtilis* and *Ralstonia pickettii* have developed strategies, such as biosorption, bioaccumulation and biotransformation, that reduce significantly the bioavailability of environmental contaminants (Singh, 2025). In contrast with natural or inorganic pollutant, synthetic plastics are difficult to degrade because of their feature: for many common plastics, especially polyethylene (PE), polypropylene (PP), and polystyrene (PS), the backbone is mostly constituted by carbon-carbon bonds with few or no hydrolysable groups, making direct enzymatic cleavage intrinsically difficult, limiting microbial attack. Recent studies have showed how bacteria present in the gut of some insects, like *Plodia interpunctella* and *Galleria mellonella*, are able to convert into PE in water soluble products (Mohana et al., 2020)

Despite bioremediation has a wide array of benefits and large-scale applicability, it can present a few limitations. The most relevant one is that this procedure is influenced by some abiotic factors such as temperature, pH, oxygen availability and salinity. Nevertheless, these environmental limitations can be mitigated, and the overall efficiency enhanced through two main techniques: biostimulation and bioaugmentation (Singh, 2025). Biostimulation consists in the addition of nutrients, oxygen or

substances that allow to recreate the perfect conditions for the organisms. This implementation is suitable in case of chronically contaminated sites. In contrast, bioaugmentation consists in the introduction of pollutant-specific organisms that usually are not present in that place (Matilda & Samuel, 2024). Consequentially, bioaugmentation and biostimulation coupled with new technological tools could position bioremediation as the primary sustainable solution to the huge problematic environmental pollution.

3.2 Toilet paper as the primary flushable pollutant

Waste and contaminants are not generated only by industries and factories but also by the single individual. Nowadays the global average waste generation is 494 kg per person per year, thus 3.5×10^{11} kg of waste is estimated to be generated annually only from households (Siddiqi et al., 2020). Municipal solid waste (MSW) ranged from 2.3 to 3.1 billion tons in 2019. This number is expected to grow to 2.89–4.54 billion tons by 2050 (Maalouf & Mavropoulos, 2023).

Alongside solid waste, consumption of Flushable Consumer Products (FCPs), i.e., toilet paper, tampons, and wet wipes, is steadily increasing worldwide (Beytullah & Fatih, 2021). Toilet paper, notably, is one of the major components of household waste used in the entire world: a total of 83 billion rolls is produced annually (Wang et al., 2023). Indeed, among FCPs, toilet paper is the most represented and accounts for the largest share in terms of volume (Beytullah & Fatih, 2021).

The toilet paper composition typically depends on the brand and usage requirements, but generally speaking, it is mainly made of natural cellulose fibers combined with industrial additives and functional processing chemicals. Specifically, it is almost entirely plant-derived polysaccharides, consisting of cellulose, hemicellulose and lignin averagely equal to 87% of the total composition (Palmieri et al., 2019).

The high concentration of celluloses, which is linked to the necessity of softness, high wet strength and absorbency, at the same time significantly reduces biodegradability (Elmas & Bekiroglu, 2019; Elmas et al.,2023). Indeed, toilet paper is one of the major pollutants of wastewater and its degradation has a huge impact on oxygen demand, biogas production, and sludge production during anaerobic digestion (Wang et al., 2023). Furthermore, non-well degraded fibers are the major contribute to pipe blockages particularly in small diameter pipes. This results in financial issues and significant public health concerns (Beytullah & Fatih, 2012). An analysis by Gülnur & Sultan, 2019 reported that residential sewerage lines, particularly in big cities, were mostly clogged with toilet papers. Moreover, annual averages of 50 000 Sanitary Sewer Overflows (SSOs) and 400,000 basement sewage backups

in basements occur as a result of pipe blockages in the United States of America (USA), and this number is increasing every year (Beytullah & Fatih, 2012).

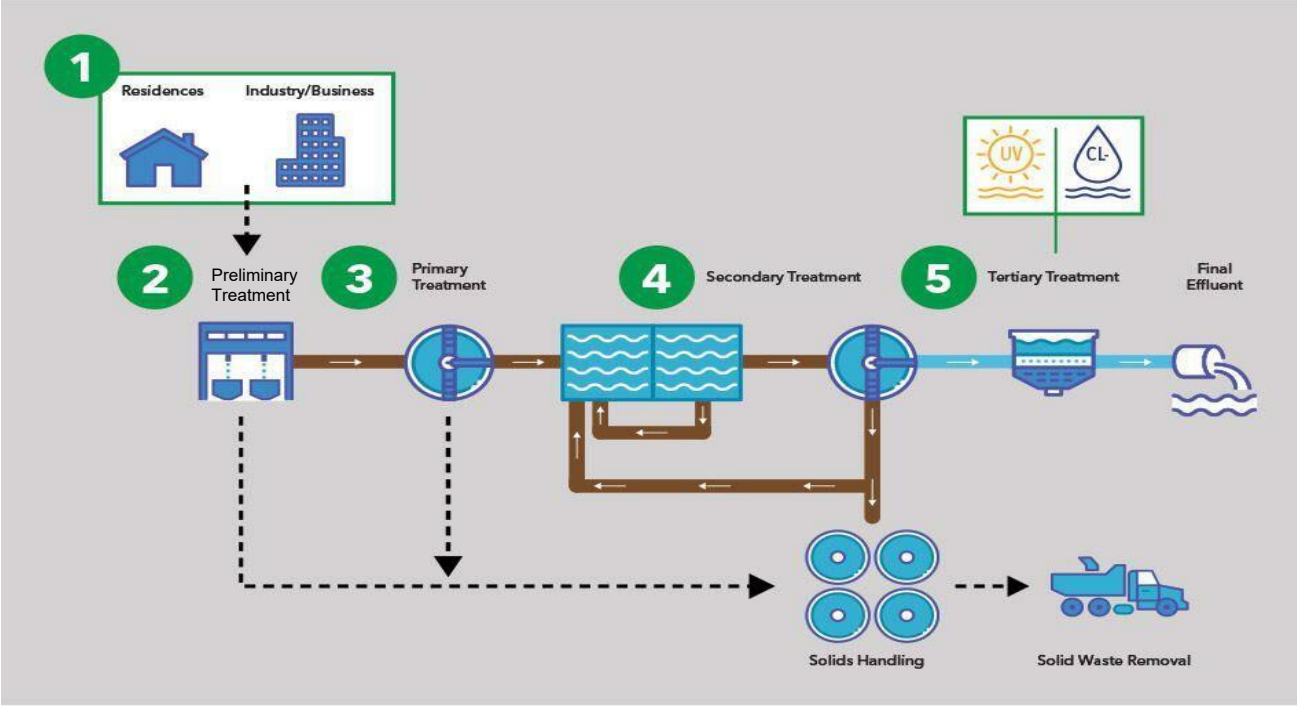


Figure 3.2 Schematic representation of the different stages of wastewater treatment. (https://www.ysi.com/applications/wastewater?srsltid=AU7gw4WNvJVH7hMHydpO3KVqpAm9YkMtsnOg2ylPh1xvLnfreIdcugta)

Figure 3.2 describes the fate of all FCPs, including toilet paper: both solid and liquid are fist translocated throw pipes, taking advantage of gravity or in some case of pumps. Subsequently, every FCP undergoes different degradation processes in wastewater treatment plant or small centralized treatment facilities buildings (Ahmed et al., 2019). Even if toilet paper goes through different purification treatments, i.e. grit screening, primary and secondary treatment processes, and sometimes advanced process some fibers remain intact (Wang et al., 2023).

To solve this problem, limited research and solutions have been so far provided. Li et al. (2020) propose the recovery of fibers from wastewater as a solution for toilet paper clogging, but it does not prevent primary pipe blockage and its economic impact. Consequently, there is the necessity of the new products that meet environment preservation and consumer expectations which are vital for long-term sustainability of wastewater collection and treatment systems (Beytullah & Fatih, 2012).

THE AIM OF THE WORK

The widespread reliance on non-degradable materials and single-use products combined with the constant global population growth poses the urgent need for sustainable ecological solutions to preserve the environment. This represents not only an industrial challenge but also a societal one, as consumers become increasingly reliant on single-use items, such as toilet paper.
Bioremediation, by taking advantage of the natural physiological traits of bacteria, seems to be the most promising option to address this issue.

This thesis aim is to provide a practical example of how one of the most extensively studied genera, *Bacillus*, and its features can be exploited for both ecological and industrial purposes. Specifically, the goal of this study is to evaluate three *Bacillus* species -*B. subtilis* (both wilde-type and engineered strains), *B. velezensis* and *B. amyloliquefaciens*- and their cellulase production and action on one of the most widely used disposable products in the world. The main goal is to integrate these strains into tissue paper manufacturing to ensure rapid substrate degradation upon disposal, thereby offering a sustainable solution to sewer pipe clogging.

Furthermore, this work highlights the synergistic collaboration between academia, specifically the University of Milan (UNIMI) and the University of Pavia (UNIPV), and industrial partners such as Kemper S.r.l. Indeed, the wild-type strains were provided by Kemper S.r.l., while the engineered strain was supplied by Professor Calvio's laboratory (Genetic of microorganisms) of the University of Pavia. All the experiments were conducted at Professor Scarì's laboratory (Nanospacelab) at the University of Milan. The final product could be an improvement of "BulkySoft active clean", the bioactive toilet paper produced by Cartiere Carrara S.p.A., one of the leading European producers of tissue.

MATERIALS AND METHODS

3.1 *Bacillus* species and strains

The following experiments were conducted using commercial preparation of wild-type *Bacillus* spp. (*B. velezensis, B. subtilis* and *B. amyloliquefaciens,* Table 3.1) with a concentration of 20 x 10^9 CFU/g. The product, composed of 20% bacterial spores and 80% sodium gluconate (excipient), was provided by Kemper S.r.l.

An engineered non-GMO strain of *B. subtilis* (Table 3.1) was additionally provided by Professor Calvio's laboratory (University of Pavia). This strain was constructed using the fully sequenced laboratory model B. subtilis 168 (specifically the JH642 derivative) as the parental background host. The strain is maintained as spores in 2xSG solid medium. As a patent application is currently under preparation, further details regarding this strain are presently undisclosed.

Species	**Strains**	**Sources**
B. subtilis	PB5946	Calvio's laboratory collection
B. subtilis	103115	Kemper S.r.l.
B. velezensis	20240430	Kemper S.r.l.
B. amyloliquefaciens	103116	Kemper S.r.l.

Table 3.1 List of *Bacillus* spp. used in the study

3.2 Culture media

LB components	**Final concentration (g/L)**	**Description**
Tryptone	10.0	Nitrogen and Peptide source
Yeast extract	5.0	Vitamins and growth factors
Sodium Chloride (NaCl)	10.0	Osmotic balance
Agar (for solid medium only)	15.0	Solidifying agent

Table 3.2 Composition Sigma Luria-Bertani (LB) Miller granulated medium [85856].
The components were solved with a proportion of 40.0 g in 1L of distilled water and then autoclaved 15 min at 121°C.

CMC agar components	Final concentration (g/L)	Description
Tryptone	10.0	Nitrogen and Peptide source
Yeast extract	5.0	Vitamins and growth factors
Sodium Chloride (NaCl)	10.0	Osmotic balance
Carboxymethylcellulose (CMC)	10.0	Carbon source and cellulose substrate
Agar	15.0	Solidifying agent

Table 3.3 Composition Sigma Luria-Bertani (LB) Miller granulated medium [85856] joined with Sodium carboxymethyl cellulose (CMC; Materiamadre, IBC ZERO S.r.l., Brescia, Italy)
The components were dissolved with a proportion of 40.0 g in 1L of distilled water and then autoclaved 15 min at 121°C.

Spizizen Minimal Medium (SMM) components	Formula (stock)	Final concentration (g/L)
Dipotassium phosphate	10.0	14.0
Monopotassium phosphate	5.0	4.0
Ammonium sulfate	10.0	2.0
Sodium citrate	10.0	1.0
Magnesium sulfate heptahydrate	15.0	0.2

Table 3.4 Composition of Spizizen Minimal Medium (SMM). The components were solved in distilled water and then autoclaved 15 min at 121°C.

2XSG medium components	Formula (stock)	Final concentration
Nutrient broth	DIFCO™ powder	16.0 g/L
Potassium chloride	KCl (powder)	2.0 g/L
Magnesium sulfate heptahydrate	$MgSO_4 \cdot 7H_2O$ (powder)	0.5 g/L
Sodium hydroxide	NaOH (1 M)	0.5 mL/L
After autoclaving and cooling to 50°C add,		
Calcium nitrate	$Ca(NO_3)_2$ (1 M)	1 mL/L
Manganese(II) chloride	$MnCl_2$ (0.1 M)	1 mL/L
Iron(II) sulfate	$FeSO_4$ (1 mM)	1 mL/L
Glucose	$C_6H_{12}O_6$ (50% w/v)	2 mL/L

Table 3.5 Composition of 2XSG medium used for spore production from *Bacillus* subtilis strain (Harwood & Cutting, 1990). After autoclaving at 121°C, 15 min and cooling to approximately 50°C, 1/1000 (v:v) of sterile stock solutions of 1 M $Ca(NO_3)_2$, 0.1 M $MnCl_2$, 1 mM $FeSO_4$ and 2 mL of 50% (w/v) $C_6H_{12}O_6$ were added aseptically.

3.3 Methods used in the study

3.3.1 Genome sequencing

The *Bacillus* spp. provided by Kemper S.r.l. were sequenced using Illumina NovaSeq 6000 at the University of Parma at GenProbio S.r.l.
The extraction of DNA was performed according to *Zymo D4300* protocol.
The sequencing libraries were prepared using the *Nextera XT Library Prep Kit* protocol.
The genome of strain PB5946 (Table 3.1) was provided by Professor Calvio.

3.3.2 In silico genomic analysis

TBLASTN searches were conducted on a virtual machine using the assembled genome sequences as local databases and the amino acid sequences of reference cellulases belonging to three subfamilies (Table 3.6) as queries. The protein sequences of the target cellulases were retrieved from the UniProt database

Enzymatic role	Protein query	Origin species
Endoglucanase (EG)	P10475 (eglS)	*B. subtilis 168*
Exoglucanase (CBH)	A8FDC4 (GH48)	*B. pumilus*
ß-glucosidase (GL)	O05508 (GH1)	*B. subtilis 168*

Table 3.6 Enzymatic role, query protein identifier, and species of origin for the three model cellulase sequences queried against the genomes of the four *Bacillus* strains analyzed in this study (sequences retrieved from UniProt, https://www.uniprot.org).

In silico Antimicrobial Resistance (AMR) profiling was performed on the assembled whole-genome FASTA sequences of each strain using the ResFinder platform hosted on the Center for Genomic Epidemiology web server (DTU, https://genepi.food.dtu.dk/services/ResFinder). Whole-genome assemblies were screened against the acquired antimicrobial resistance gene database using default search thresholds, defined as a minimum percentage identity of 90% and a minimum sequence coverage cut-off of 60%.

3.3.3 Bacteria growth

Sample preparation

For each Kemper S.r.l. *Bacillus* strains, 0,01 g of spore powder was suspended in 10 mL of sterilized physiological saline solution (9 g/L NaCl), contained in a 15mL sterile Falcon tube, previously sterilized. Serial dilutions were prepared from the stock suspension. 100 µL from each dilution were withdrawn and plated onto 20 mL LB agar contained in a 9 cm diameter Petri dish. The spores of the engineered *B. subtilis* strain were directly spread onto LB agar. All four strains were incubated overnight at 37 °C.

Following incubation, a single colony from each strain was selected and inoculated in 4 mL of LB broth contained in a 15 mL Falcon tube, plugged with sterilized cotton and incubated overnight at 37 °C with shaking at 150 rpm.

The following day, 25 µL from each inoculum was added to 20 mL of LB broth in a 100 mL Erlenmeyer flask plugged with sterilized cotton and incubated at 37 °C with shaking at 150 rpm, for the required time.

Spectrophotometric Analyses

Optical density measurements at 600 nm (OD_{600}) were performed using the GENESYS 150 UV-Vis Spectrophotometer (Thermo Fisher Scientific, Waltham, MA, USA).

Every hour, 0,9 mL aliquots were withdrawn from each culture, transferred into 1,5 mL Microcentrifuge tubes and fixed with 0,1 mL of 4% (w/v) paraformaldehyde (PFA) in 0.1 M phosphate-buffered saline (PBS). A mixture of 0,9 mL uninoculated LB broth and 0,1 mL of the PFA/PBS fixative was used as the reference blank.

The data collected during the experiment were used to obtain the growing curve of each strain. From the curve, Excel analyses were conducted, obtaining the Equation curve ($y = A \cdot e^{\mu x}$) of each growing strain, the Growth rate (μ; h^{-1}) and the Duplication Time (T_d; h), calculated with the following formula:

$$T_d = \frac{\ln(2)}{\mu}$$

Flow Cytometric Analyses

Flow cytometer analysis was performed using BD Accuri™ C6 Plus flow cytometer (BD Biosciences, San Jose, CA, USA).

Every 1h, 5h and 10h, a 0,9 mL aliquot was withdrawn from each culture, transferred into 1,5 mL microcentrifuge tubes and fixed with 0,1 mL of 4% PFA in 0,1 M PBS.

A solution containing 0,9 mL of uninoculated LB broth and 0,1 mL of the PFA/PBS fixative served as the blank.

The flow cytometry analyses were complete by using Floreada.io (https://floreada.io).

3.3.4 Congo Red Assay

The Congo red assay was carried out in two distinct operational approaches: by depositing either cultured bacterial samples or the enzyme-rich supernatant.

Cultured bacteria samples preparation

Sample preparation, serial dilutions, and agar plating were carried out as previously detailed in Section 3.3.3. A 1 mL sample of each culture was then collected and were adjusted to an equal initial density (OD_{600}) using distilled water prior to the assay.
Subsequently, 2µl of each standardized bacterial suspension was spotted onto a 20 mL CMC agar contained in 9 cm diameter Petri dish. The plates were incubated at 37 °C for 24h.

Cellulase-reach supernatant preparation

Bacterial sample preparation and plating were performed following the exact procedure described above in Section 3.3.3 (Sample preparation). Thereafter, a single colony for each strain is selected, mixed with 1 mL of sterilize physiological saline solution (0,9% NaCl) and inoculated into 20 mL of LB broth in a 100 mL Erlenmeyer flask fitted with a sterile cotton plug. Cultures were incubated overnight at 37 °C under shaking (150 rpm).
The cell-free supernatant was harvested by centrifugation at 10 000 rpm for 10 min. To remove possible bacteria leftover, the supernatant was filtrated with 0,22 µm PES membrane filter. 50 µl aliquots of the filtered supernatant of each sample were injected in wells created in the CMC agar. Finally, the plates were incubated at 37 °C for 36 h.

Congo red assay execution

Upon completion of the incubation period, 20 mL of 0,1% (w/v) Congo red solution was poured onto the Petri dish and allowed to react for 30 min. The excess dye was discarded and 20 mL of 1 M NaCl solution was added into the plate for 20 min detaining step. This last step was repeated twice to ensure the complete removal of unbound dye and background staining.
Clear halos around the colonies or wells became visible, and their outer diameters were measured. The Enzymatic Index (EI) was calculated according to the following formula (Balla et al., 2022):

$$EI = \frac{dH - dC}{dC}$$

where, EI is the Enzymatic Index, the dH is the total diameter of the hydrolysis halo (mm) and the dC is the diameter of the colony or well (mm). To determine the dimensions of both the halo and the colony, plate images were analyzed using ImageJ, setting a ruler as a spatial scale reference.

3.3.5 Scanning Electron Microscopy (SEM) analysis

Sample preparation

Bacterial suspensions were prepared and plated as previously described (Section 3.3.3). Subsequently, each sample was centrifuge at 10 000 rpm for 10 min. The resulting pellet was resuspended in 2mL of sterilized physiologic solution (0,9% NaCl). To ensure a uniform initial cell density across all samples, optical density at 600 nm (OD_{600}) was measured, and concentrations were adjusted using sterilized physiologic solution (9% NaCl).

The inoculum of each strain was added at 4 mL of SMM medium in each of well of 6-well-plate containing a sterilized 1 cm x 1cm piece of paper. The paper substrate used in this experiment and in the subsequent one was a 2-ply tissue paper with a basis weight of 18 g/m², kindly provided by Cartiere Carrara. Control wells containing uninoculated medium with paper (control) and medium alone (blank) were set up in parallel. All samples were incubated for the required time at 37°C with shaking at 150 rpm. To prevent medium evaporation, the 6-well-plates were sealed with Parafilm and placed inside a humidified chamber.

Sample fixation

Paper specimens from each sample were collected after 1, 3 and 7 days of incubation.

Each paper was gently rinsed twice in sterile distilled water and then submerged in a paraformaldehyde-glutaraldehyde (PAFG) fixative solution for 20 min at root temperature. Immediately after, three consecutive washes in distillated water for 3 min each were performed.

he samples were dehydrated through a 7-min incubation in 5 mL of a graded ethanol series (50%, 70%, 80%, 90%, and 100% v/v). The final dehydration step in 100% ethanol was repeated twice. To complete the chemical drying, the paper pieces were submerged for 7 min first in a 1:1 (v/v) mixture of hexamethyldisilazane (HMDS) and absolute ethanol, followed by immersion in 100% HMDS for 7 min. The samples were subsequently allowed to dry air overnight under a laminar flow hood.

The samples were subsequently allowed to dry air overnight under a laminar flow hood.

Sputter Coating and SEM Imaging

Prior to SEM evaluation, each dried paper was mounted onto an aluminum stub using double-side conductive carbon tape and sputter-coated with silver using a Leica EM ACE600 high-vacuum coater (Leica Microsystems, Wetzlar, Germany) to prevent surface charge accumulation.
The Scanner Electron Microscopy analysis was performed by using a Leo 438 VP SEM (Carl Zeiss AG, Oberkochen, Germany) operating under high vacuum conditions.

3.3.6 Paper weight loss

Sample preparation

Preparation and plating of the bacterial suspensions followed the protocol detailed in Section 3.3.3. Following incubation, each culture was centrifuged at 10,000 rpm for 10 min. The resulting pellet was resuspended in 2mL of sterilized physiologic solution (0,9% NaCl). To ensure a uniform initial cell density across all samples, optical density at 600 nm (OD_{600}) was measured, and concentrations were adjusted using sterilized physiologic solution (0,9% NaCl).

The standardized bacteria inoculum of each strain was added to 5 mL SMM medium in a 6 cm diameter Petri dishes containing a the same type of piece of paper described previously. The papers were previously dry in a laboratory oven at 80°C overnight. Then, they were weighted with an analytical balance (Entris 224-1S; Sartorius AG, Göttingen, Germany) with an accuracy of 0.1 mg and sterilized through ozonation for 30 min.

Control plates (uninoculated medium with paper) and blank plates (medium alone) were prepared in parallel.

All samples were incubated at 30°C for the designed time intervals. To prevent medium evaporation, the Petri dishes were put inside a humidified chamber.

Mass Loss Measurement

Paper specimens from each treatment (including any recovered fragment) were collected after 1, 3, and 7 days of incubation. Each sample was gently rinsed three times with 20 mL of pre-warmed (50 °C) sterile distilled water to remove residual medium components and loosely attached biomass. Subsequently, the paper samples were dried in a laboratory oven at 60 °C overnight. After drying, the final dry mass of each sample was recorded using the same analytical balance.

The percentage of paper mass loss (%ΔW) was calculated using the following formula:

$$\%\Delta W = \frac{W_0 - W_t}{W_0} x100$$

Where W_0 is the initial dry weight of the paper sample (mg) and W_t is the dry weight after incubation (mg). From this data was possible to obtain the Net $\%\Delta W$, resulting as:

$$Net\ \%\Delta W = \%\Delta W_{sample\ with\ bateria} - \%\Delta W_{controll}$$

All assays were performed in triplicate.

RESULT AND DISCUSSION

4.1 Bioinformatic genomic screening of cellulolytic enzymes and Antimicrobial Resistance (AMR) profiling

Preliminary TBLAST genomic analysis was conducted to assess the present of cellulase genes in the selected *Bacillus* strains. The reference sequences for the three primary cellulase classes were: endoglucanase (P10475), exoglucanase (A8FDC4), and β-glucosidase (O05508). the percentage identities are summarized in the heatmap (Figure 4.1), while full bioinformatic parameters (% coverage and E-values) are detailed in Table 4.1.

Query	Genome target	% Identity	% Coverage	E-value
Endoglucanase (P10475)	Engineered *B. subtilis*	100	100	0
Exoglucanase (A8FDC4)	Engineered *B. subtilis*	N.S.	0	N.S.
ß-glucosidase (O05508)	Engineered *B. subtilis*	99,785	100	0
Endoglucanase (P10475)	*B. subtilis*	97,4	100	0
Exoglucanase (A8FDC4)	*B. subtilis*	N.S.	0	N.S.
ß-glucosidase (O05508)	*B. subtilis*	98,71	100	0
Endoglucanase (P10475)	*B. velezensis*	93,174	99	0
Exoglucanase (A8FDC4)	*B. velezensis*	N.S.	0	N.S.
ß-glucosidase (O05508)	*B. velezensis*	81,739	100	0
Endoglucanase (P10475)	*B. amyloliquefaciens*	93,387	100	0
Exoglucanase (A8FDC4)	*B. amyloliquefaciens*	57,143 (N.S.)	20	2,9
ß-glucosidase (O05508)	*B. amyloliquefaciens*	82,174	100	0

Table 4.1 TBLASTN alignment metrics (percentage sequence identity, query coverage, and E-value) for reference cellulase queries against the target *Bacillus* genomes. (N.S. = Not Statistically Significant, E-value > 1,0). For raw alignment outputs, see Section I ("TBLAST genomic analysis raw data") in the Supporting Materials.

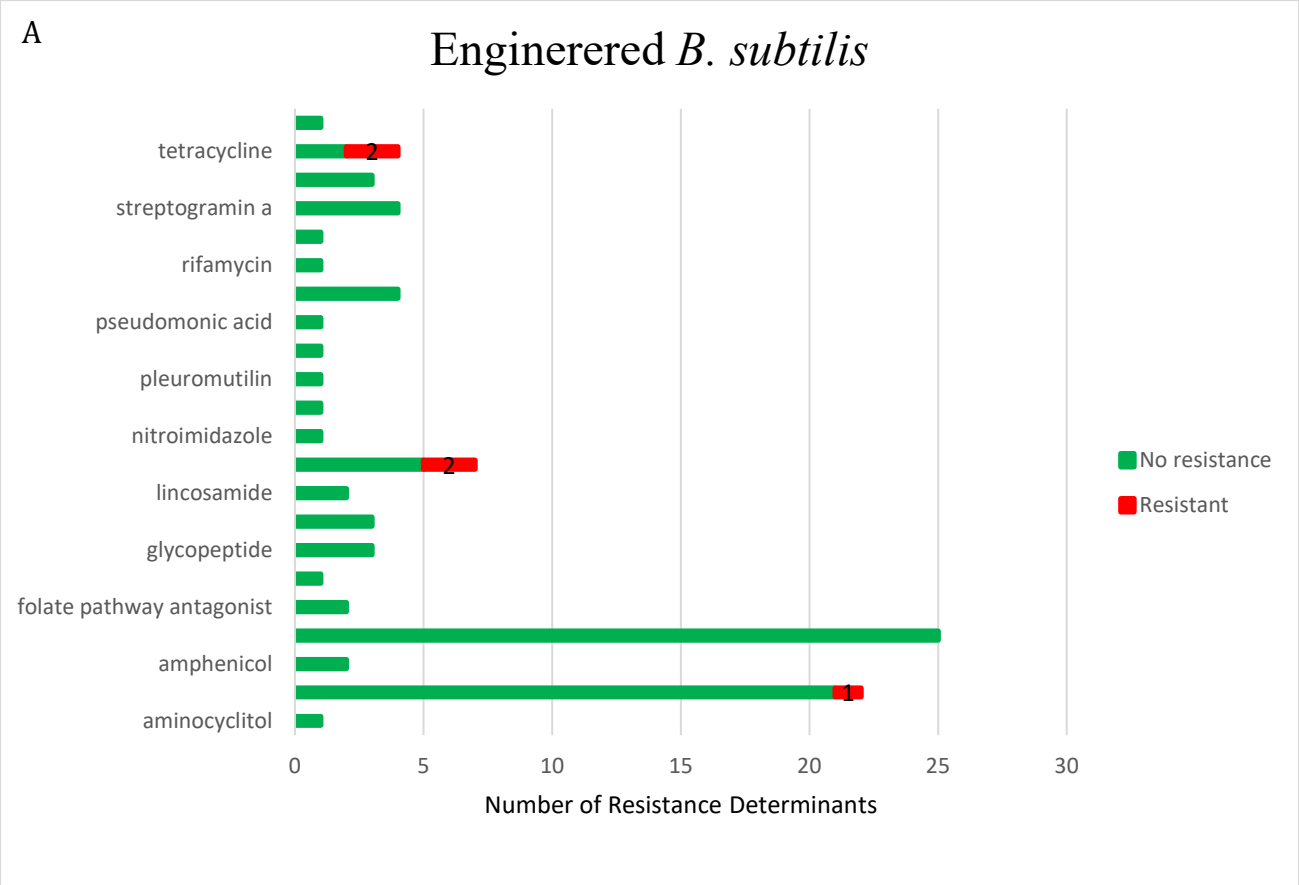


Figure 4.1 Sequence identity heatmap (%) of model cellulases aligned against the four Bacillus genomes (N.-S. = non-significant match). For raw alignment outputs, see Section I ("TBLAST genomic analysis raw data") in the Supporting Materials.

Both endoglucanase and β-glucosidase genes were successfully identified in all four genomes with high statistical significance. Endoglucanase exhibited high sequence conservation across all strains. Similarly, β-glucosidase showed near-perfect identity in *B. subtilis strains* (> 98,7%) and substantial conservation in *B. velezensis* (81,7%) and *B. amyloliquefaciens* (82,2%).

Instead, no statistically significant alignments were detected for exoglucanase across any of the genomes (E-value > 2,8, coverage ≤ 20%). This result is reliable with the literature, indicating that *Bacillus* species typically lack dedicated exoglucanases.

Additionally, in silico antimicrobial resistance (AMR) screening was conducted on the whole-genome sequences of the candidate *Bacillus* strains to evaluate their biosafety profile prior to industrial integration (Figures 4.2)



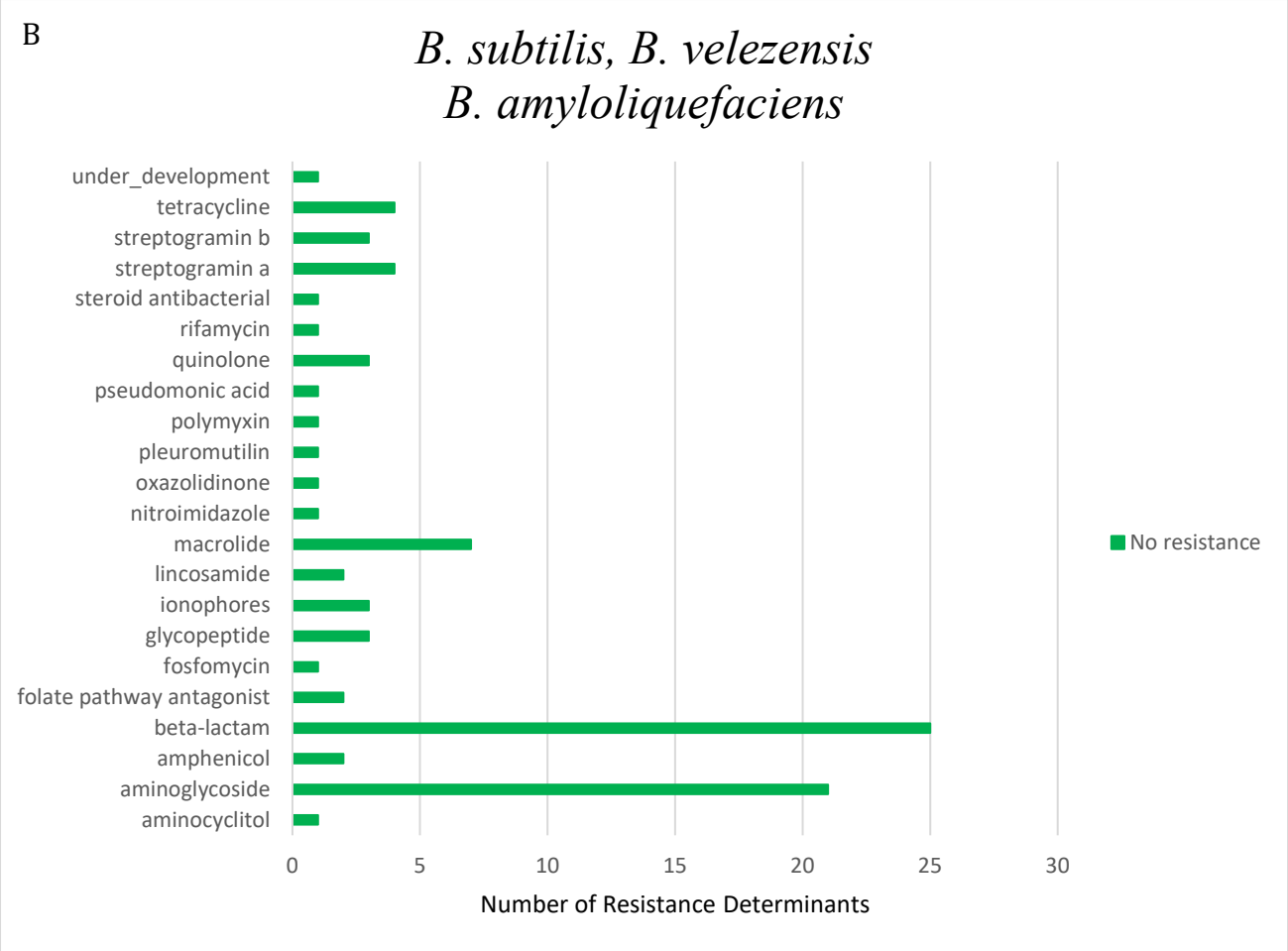


Figure 4.2 In silico antimicrobial resistance (AMR) profiles of the analyzed *Bacillus* strains. (A) Engineered *B. subtilis*, showing resistance determinants for aminoglycoside, macrolide, and tetracycline classes; (B) Representative susceptibility profile of wild-type strains (*B. subtilis, B. velezensis*, and *B. amyloliquefaciens*), all displaying complete absence of resistance genes. For raw alignment outputs, see Section II ("Antimicrobial resistance screening raw data") in the Supporting Materials.

The wild-type strains (*Bacillus subtilis*, *Bacillus amyloliquefaciens*, and *Bacillus velezensis*) exhibited a complete absence of predicted resistance genes across all tested antibiotic classes (100% susceptibility profile). This demonstrates a clean genetic background, confirming their high biosafety standard for environmental applications.

Conversely, the engineered *B. subtilis* strain revealed the presence of specific resistance determinants belonging to three distinct antibiotic classes: aminoglycosides, macrolides, and tetracyclines. The remaining 19 antibiotic classes showed no resistance hits.

The detection of these resistance genes in the engineered strain does not imply a biosafety risk, as *B. subtilis* is a non-pathogenic, Qualified Presumption of Safety (QPS) organism.

In accordance with EFSA guidelines regarding microorganisms introduced into the environment, antimicrobial resistance profiles must be evaluated to exclude Horizontal Gene Transfer (HGT) risks via Mobile Genetic Elements (MGEs). In this regard, the engineered strain was developed from the fully sequenced and well-characterized laboratory background *B. subtilis* 168 (specifically strain JH642), with no exogenous resistance genes or selection markers introduced during genetic engineering.

Consequently, the identified resistance hits represent strictly endogenous, chromosomal features native to the host genome. Because these determinants are non-mobile and intrinsic, they pose no potential for gene transfer to gut microbiota or environmental pathogens, fully satisfying EFSA biosafety criteria for environmental applications.

4.2 Comparative growth kinetics and flow cytometric validation of *Bacillus* strains

To evaluate and compare the physiological performance and replication kinetics of the selected Bacillus strains, cell growth was monitored over a 24-hour incubation period. Optical density measurements (OD_{600}) were collected at regular intervals to establish semi-logarithmic growth curves and determine the specific growth rates (μ) during the exponential phase.

The comparative growth profiles for all four strains are presented in Figure 4.3:

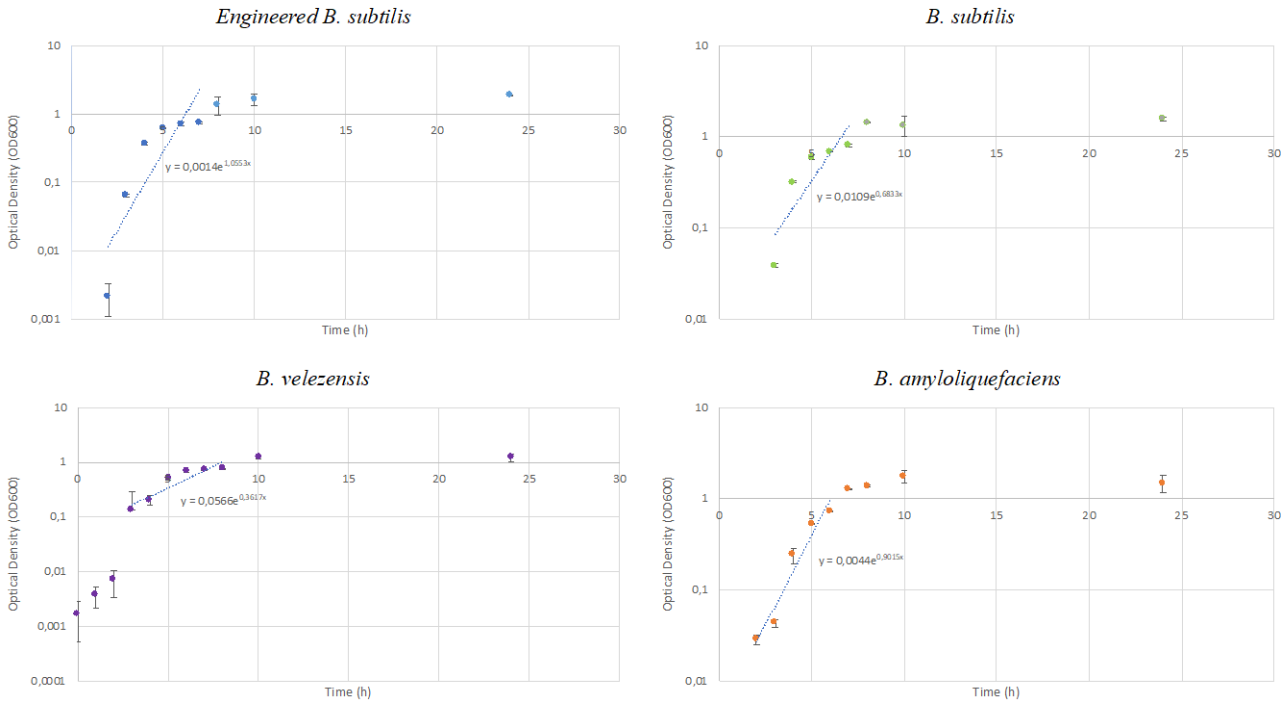


Figure 4.3 Growth curves of the four *Bacillus* strains plotted on a semi-logarithmic scale (OD_{600} as a function of time). For *B. velezensis*, the initial time points (t = 0–2 h) were excluded from the exponential growth rate calculation as they represent the lag phase (OD_{600} <0.01)

All four profiles exhibit the characteristic phases of bacterial growth, including a distinct exponential phase and a subsequent stationary phase. All the strains seem to arrest their exponential growth and reach the stationary phases between 7 and 10 h of incubation, stabilizing at maximum optical densities (OD_{600}) between 1.2 and 2.0. A short or virtually undetectable lag phase was observed across the strains.

The aim of this experiment was to evaluate the timing and possible differences in growth behavior of the four strains to understand their physiological adaptation under identical culture conditions and to define the optimal cell density window for downstream enzymatic production.

To provide a more comprehensive overview, Growth rate (μ; Figure 4.4) and Duplication time (Td; Figure 4.5) were also analyzed.

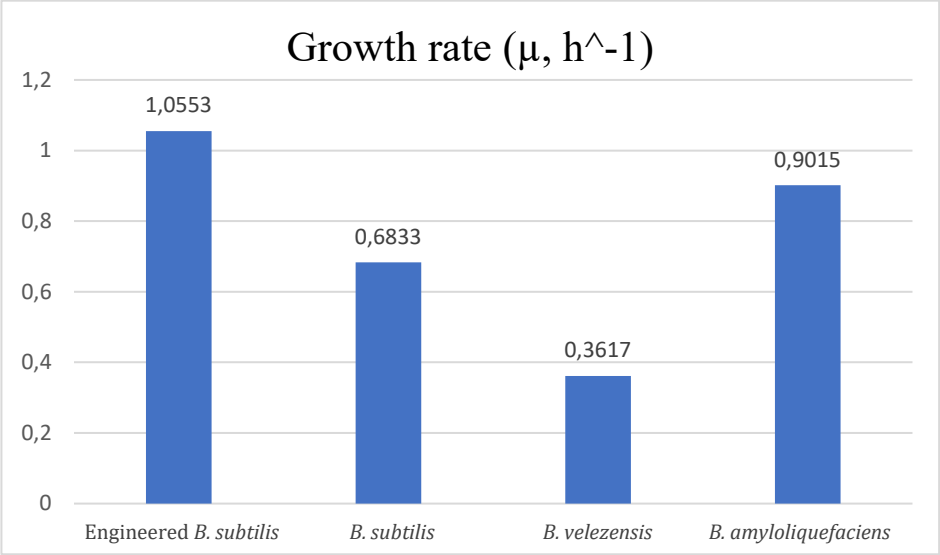


Figure 4.4 Specific growth rates (μ) of the four Bacillus strains evaluated during exponential growth.

Regarding the for Growth rate (Figure 4.2), a distinct difference is present: the Engineered *B. subtilis* exhibited the highest growth rate (μ = 1,055 h^{-1}), followed by *B. amyloliquefaciens* (μ = 0,902 h^{-1}), wild-type *B. subtilis* (μ = 0,683 h^{-1}), and *B. velezensis* (μ = 0,362 h^{-1}). Notably, the lack of differences between the engineered *B. subtilis* and its wild-type version confirms that the genetic engineering did not induce a noticeable metabolic change. Instead, the lower growth rate of *B. velezensis* highlights distinct species-specific physiological adaptations.

To complement the growth rate analyses, the cell doubling time (Td) during the exponential phase was calculated for each strain (Figure 4.5).

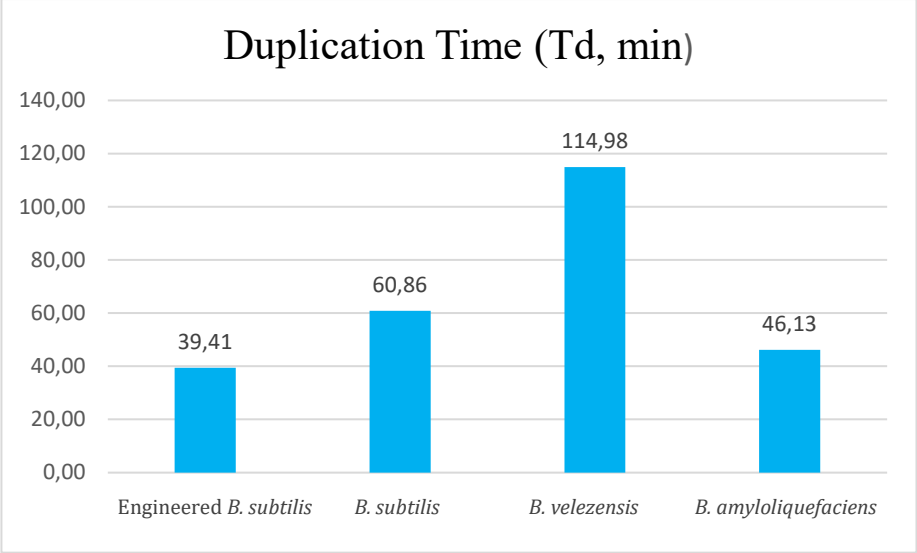


Figure 4.5 Specific duplication time (Td) of the four Bacillus strains evaluated during exponential growth.

In accordance with the growth rate, the engineered *B. subtilis* demonstrated the shortest doubling time (Td = 39,41 min), whereas the wild-type *B. subtilis* exhibited a doubling time of 60,86 min.
B. *amyloliquefaciens* showed a comparably rapid generation time (Td = 46,13 min), whereas *B. velezensis* required a substantially longer time to double its biomass (Td = 114,98 min), reflecting fundamental differences in cell division kinetics among the investigated species.

Lastly, to validate optical density (OD_{600}) as a proxy for bacterial concentration, a comparative correlation analysis was performed against flow cytometry cell counts across three key time points: 2 h, 5 h (exponential phase), and 10 h (early stationary phase) (Figure 4.6). While optical density correlates strongly with cell counts during active exponential proliferation ($t \leq 5$ h), entering the stationary phase at 10 h leads to lower overall determination coefficients for *B. velezensis* (R^2 = 0,7464) and engineered *B. subtilis* (R^2 = 0,7178). As cultures reach stationary phase, starvation induces significant morphological shifts, including cell shrinkage and the onset of sporulation. Because smaller, stationary-phase cells exhibit altered light scattering properties per cell compared to exponentially growing cells, total turbidity (OD_{600}) no longer maintains a strict linear relationship with physical cell counts.

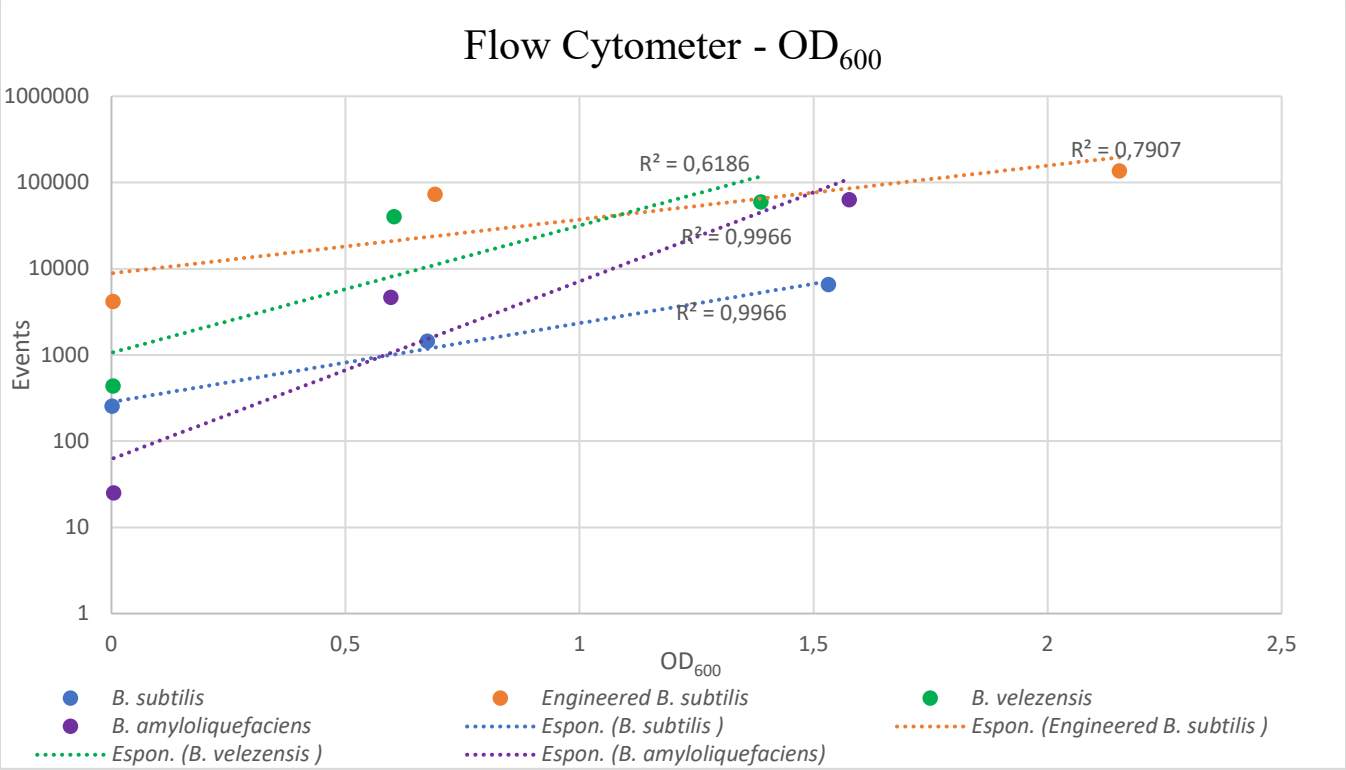


Figure 4.6 Correlation between optical density (OD_{600}, linear scale) and flow cytometry event counts (logarithmic scale) for the four *Bacillus* strains.

4.3 Congo red agar diffusion demonstrates enhanced cellulase secretion in the engineered *B. subtilis*

To evaluate the cellulolytic capability of bacterial strains, a semi-quantitative Congo Red agar assay was performed on carboxymethylcellulose (CMC) media. The resulting plates are reported in Figure 4.7, (A) for bacteria culture assay and (B) for supernatant assay.

Based only on qualitative evaluation is notable that the discrepancy between *B. subtilis*, both engineered and wild-type, as regards plate contents bacteria colonies and only engineered *B. subtilis* in plate with supernatant.

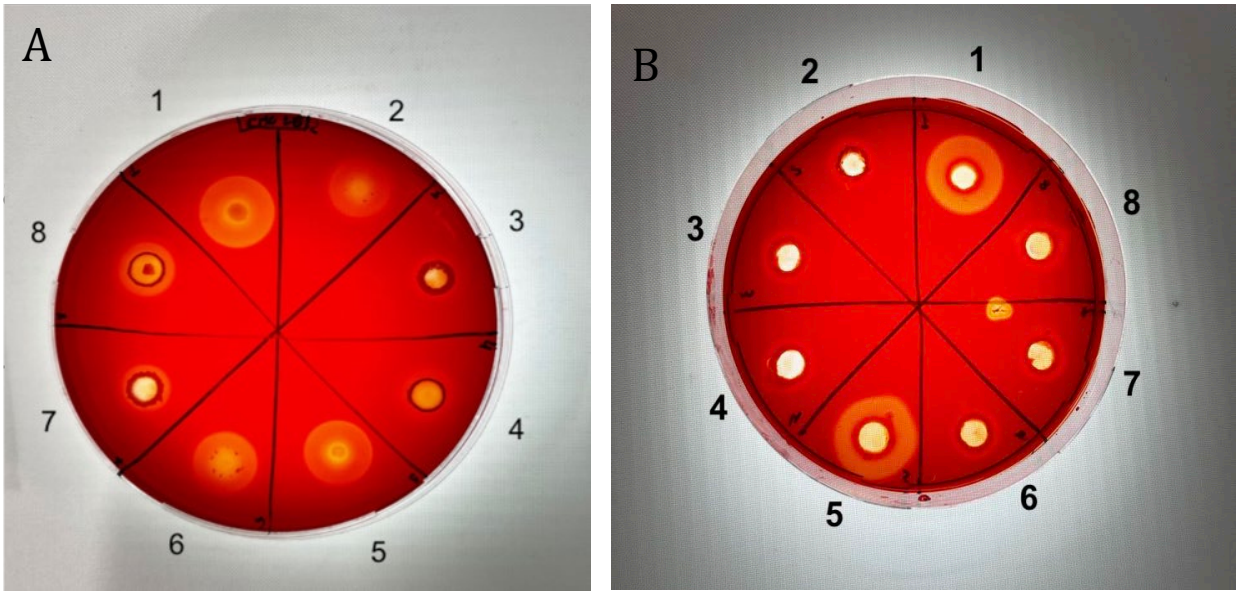


Figure 4.7 Qualitative Congo Red agar diffusion assay on carboxymethylcellulose (CMC) medium evaluating cellulolytic activity. (A) Bacterial culture spots. (B) Cell-free culture supernatants. The duplicate spots for each tested strain correspond to: 1 and 5, engineered *B. subtilis*; 2 and 6, wild-type *B. subtilis*; 3 and 7, *B. velezensis*; 4 and 8, *B. amyloliquefaciens.*

In addition, semi-quantitative analysis was conducted based on enzymatic index (Figure 4.8 and 4.9).

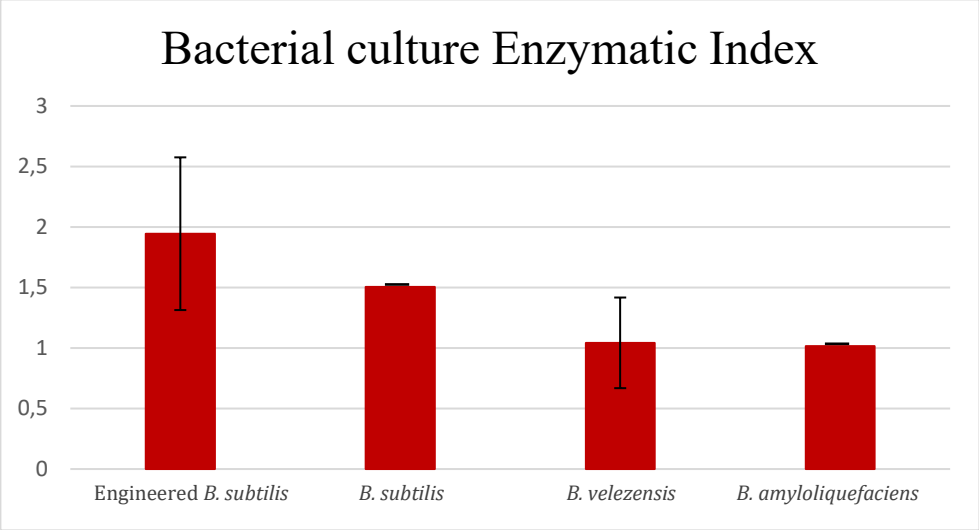


Figure 4.8 Enzymatic Index (EI) of intact bacterial cultures evaluated via Congo Red assay on CMC agar plates. Values represent the ratio of the halo diameter to colony diameter. An EI > 1,0 denotes functional extracellular cellulolytic activity.

Engineered *B. subtilis* exhibited the highest cellulolytic performance among all tested strains, reaching a mean Enzymatic Index of 1,95, which markedly exceeded that of the wild-type *B. subtilis* (EI = 1,51). Conversely, *B. velezensis* and *B. amyloliquefaciens* displayed minimal halo formation beyond the colony perimeter, yielding EI values close to baseline (EI = 1,05 and EI = 1,02, respectively). These findings demonstrate that genetic engineering significantly enhanced extracellular endoglucanase expression and secretion in *B. subtilis*, enabling superior in situ degradation of cellulosic polymers.
Concerning the assay performed with the culture cell-free supernatants, the quantitative analysis supernatant assay (Figure 4.9) directly mirrored the qualitative clearance observed on CMC agar plates (Figure 4.7B).

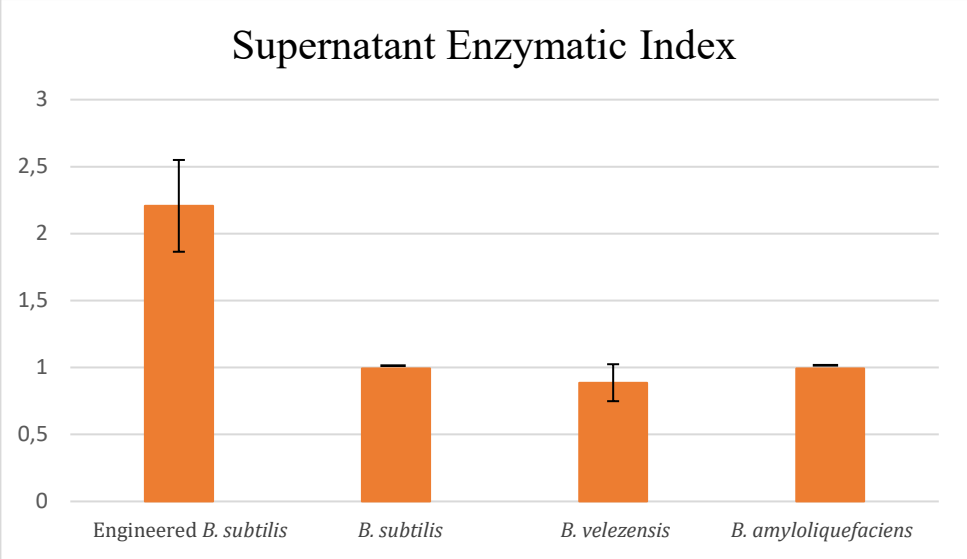


Figure 4.9 Enzymatic Index (EI) of cell-free supernatants evaluated via Congo Red assay on CMC agar plates. Values represent the ratio of halo diameter to colony diameter. An EI > 1,0 denotes functional extracellular cellulolytic activity.

Also in this case, the engineered *B. subtilis* show an extremely high cellulase secretion (EI = 2,2). This result demonstrates that the recombinant endoglucanase is efficiently secreted into the extracellular environment and retains robust catalytic activity independent of cell viability. In contrast, the cell-free supernatants of wild-type *B. subtilis, B. velezensis,* and *B. amyloliquefaciens* showed no detectable enzymatic halo beyond the well perimeter (EI ≤ 1,00).

4.4 SEM analysis reveals microstructural degradation and fiber truncation

To visually assess bacterial colonization, surface attachment, and paper degradation over time, identical samples of toilet paper were incubated with bacteria, and Scanning Electron Microscopy (SEM) was performed at 24 h, 3 days, and 7 days of incubation (Figure 4.9). This is a qualitative experiment; quantitative results are analyzed in the following chapter.

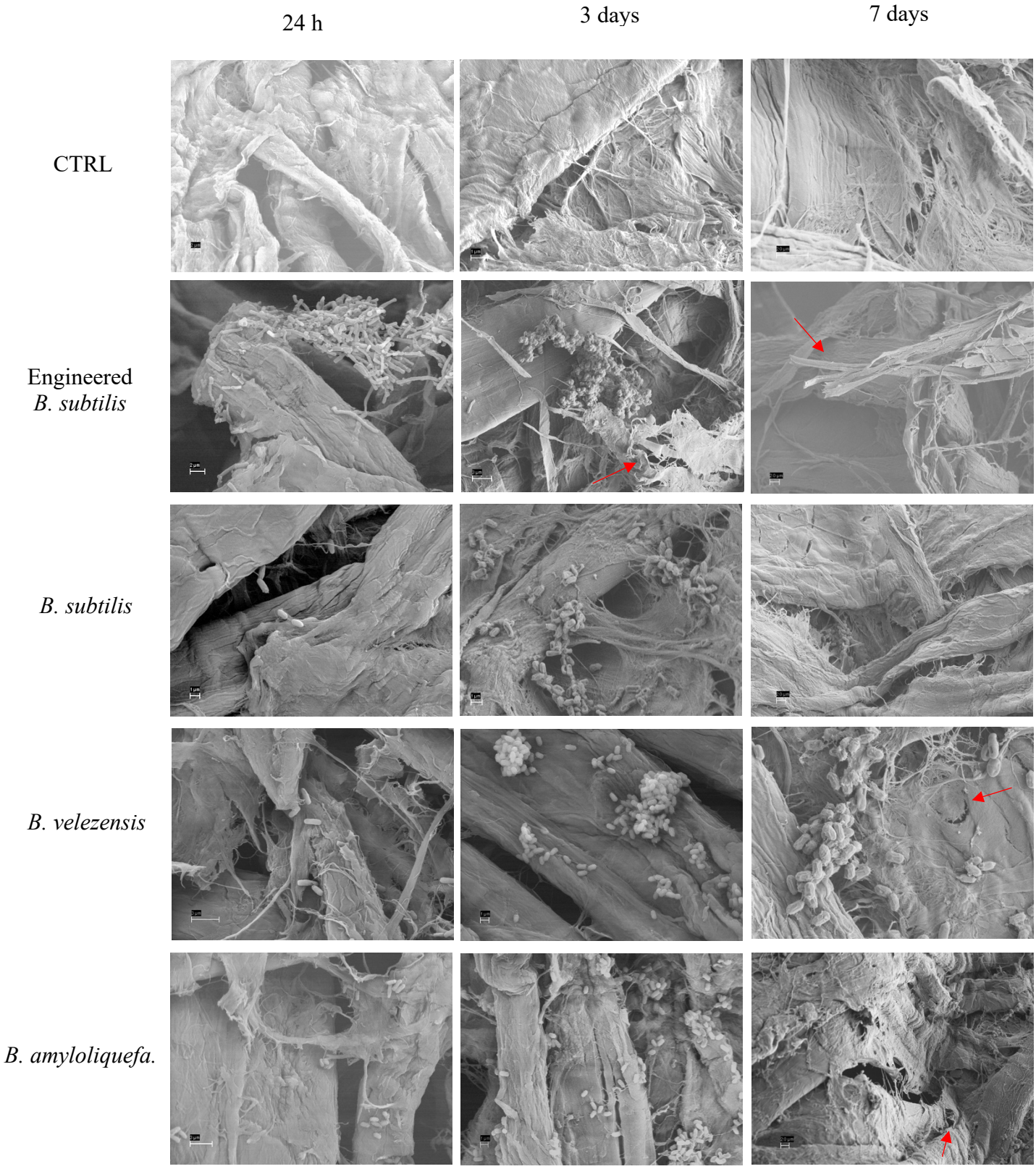


Figure 4.10 Scanning Electron Microscopy (SEM) micrographs illustrating paper fiber colonization and degradation by *Bacillus* strains over time (24 h, 3 days, and 7 days). Red arrows underlined fibers degradation.

Uninoculated control samples (CTRL, only SMM medium and paper) maintained smooth, intact cellulose fibers with well-defined microfibrillar networks throughout the 7-day period. In contrast, all bacterial strains displayed successful attachment to the paper substrate, with differences in colonization patterns and degradation impact.

The engineered *B. subtilis* demonstrated the most aggressive substrate degradation. By 24 h, dense bacterial networks coated the fibers. By day 3, significant microfibrillar disintegration and matrix softening were evident (Figure 4.9, red arrow). By day 7, extensive enzymatic erosion resulted in severe fiber thinning, surface pitting, longitudinal delamination, and complete structural truncation/snapping of cellulose fibers (Figure 4.9, red arrow). Notably, no intact bacterial cells were detected on day 7, which could be attributed to extensive cell lysis following nutrient exhaustion in late stationary phase, as well as loss of unanchored biomass during the washing and dehydration steps of SEM sample preparation once the supporting matrix collapsed.

At 24 h, wild-type *B. subtilis* displayed individual rod-shaped cells adhering along the longitudinal axis of the fibers. By day 3, bacterial density increased, forming small micro-colonies anchored primarily within the cellulosic matrix. By day 7, wild-type B. subtilis established consistent surface colonization accompanied by a thin, uniform biofilm layer across the fiber trunk. Although a slight increase in surface roughness was noticed, the overall structural continuity and integrity of the individual cellulose fibers remained almost preserved, with no evidence of fiber snapping, deep pitting, or microfibrillar delamination.

In the case of *B. velezensis,* the initial attachment at 24 h was minimal, with only isolated bacilli scattered across the fiber surface. By day 3, the strain organized into dense, localized cell clusters characterized by aggregated rod-shaped bacilli embedded within the fiber network. By day 7, this dense cellular aggregation persisted: a localized surface rupture formed directly under the bacterial clusters (Figure 4.9, red arrow).

Similarly, *B. amyloliquefaciens* exhibited limited initial adherence at 24 h, followed by a huge expansion of extracellular polymeric substances (EPS) by day 3, which effectively covered the cellulose fibers. By day 7, EPS matrix created extensive biological inter-fiber bridges. In this way, local enzymatic activity together with matrix tension created visible cracks and tears in the paper

network (Figure 4.9, red arrow). Nevertheless, unlike the heavy degradation seen in engineered *B. subtilis*, the main fiber structure remained intact under the biofilm.

It is noted that these ultrastructural observations serve as a qualitative assessment of fiber colonization and physical damage; rigorous quantitative metrics regarding substrate hydrolysis and degradation kinetics are detailed in the subsequent chapter.

4.5 Gravimetric weight loss analysis of cellulosic substrates

To evaluate the cellulolytic efficiency of the selected Bacillus strains, cellulosic paper samples were incubated with bacterial cultures alongside uninoculated controls. Paper breakdown was monitored over a 7-day period through both qualitative visual observation and quantitative dry weight loss measurement.

The macroscopic appearance of the paper substrate after 3 and 7 days of incubation is shown in Figure 4.11:

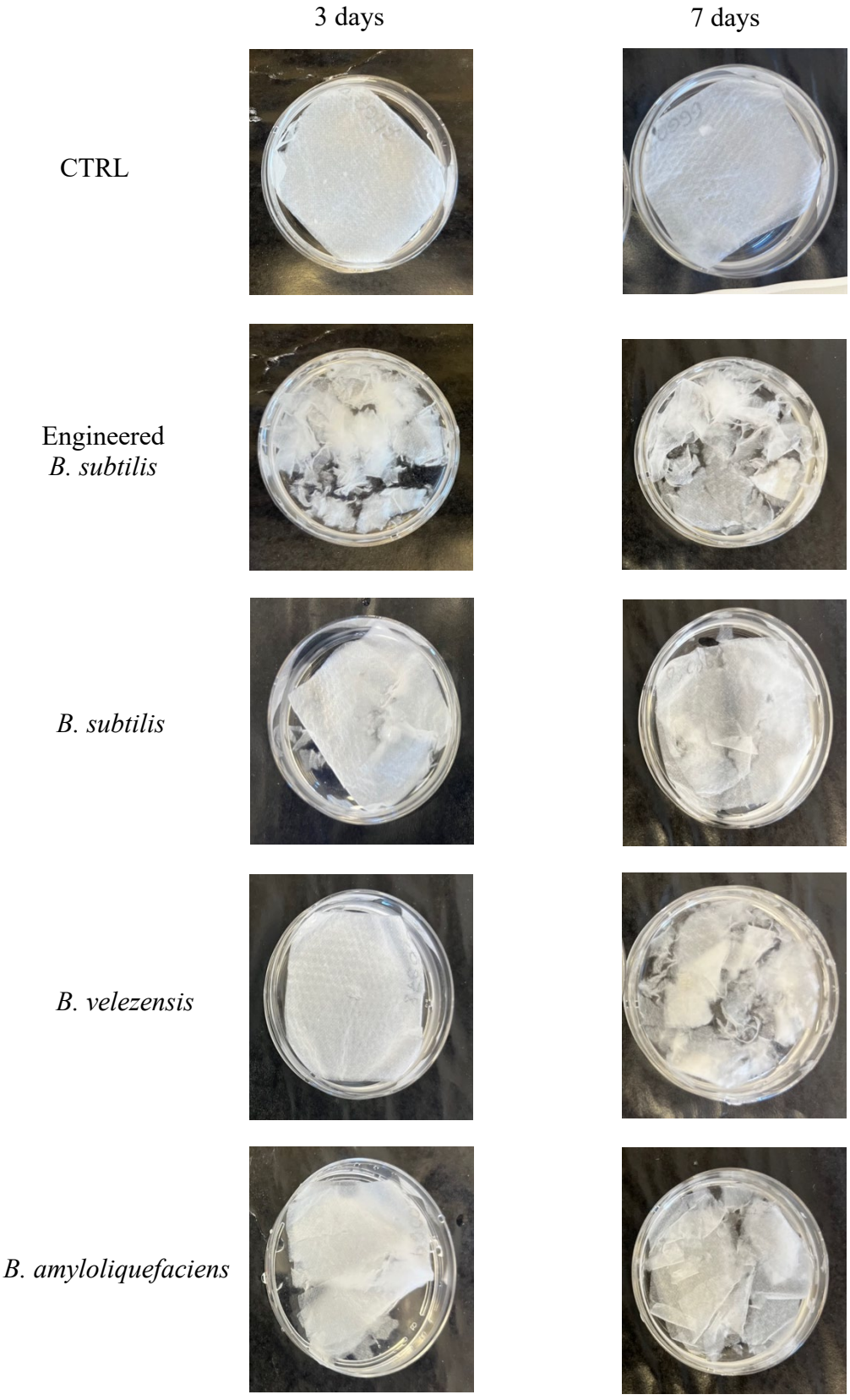


Figure 4.11: Macroscopic evaluation of cellulosic paper substrate degradation after 3 and 7 days of incubation with different Bacillus strains compared to the uninoculated control (CTRL).

The control (CTRL) preserved its structure and integrity throughout the entire 7-day incubation period, confirming that paper breakdown was strictly biogenic rather than abiotic or mechanical.

Among all tested strains, the engineered *Bacillus subtilis* seemed to exhibit superior degradative capacity, causing total structural collapse as early as day 3. The wild-type strains *B. velezensis* and *B. amyloliquefaciens* demonstrated a progressive degradation pattern, characterized by edge fraying at day 3 and extensive matrix fragmentation by day 7. Conversely, wild-type *B. subtilis* displayed a more conservative effect, without achieving full structural disruption within the tested timeframe.

These macroscopic observations are totally qualitative, thus to quantify the kinetics of cellulose depolymerization, the net percentage dry weight loss of paper pieces was tracked over 1, 3, and 7 days of incubation (Figure 4.10).

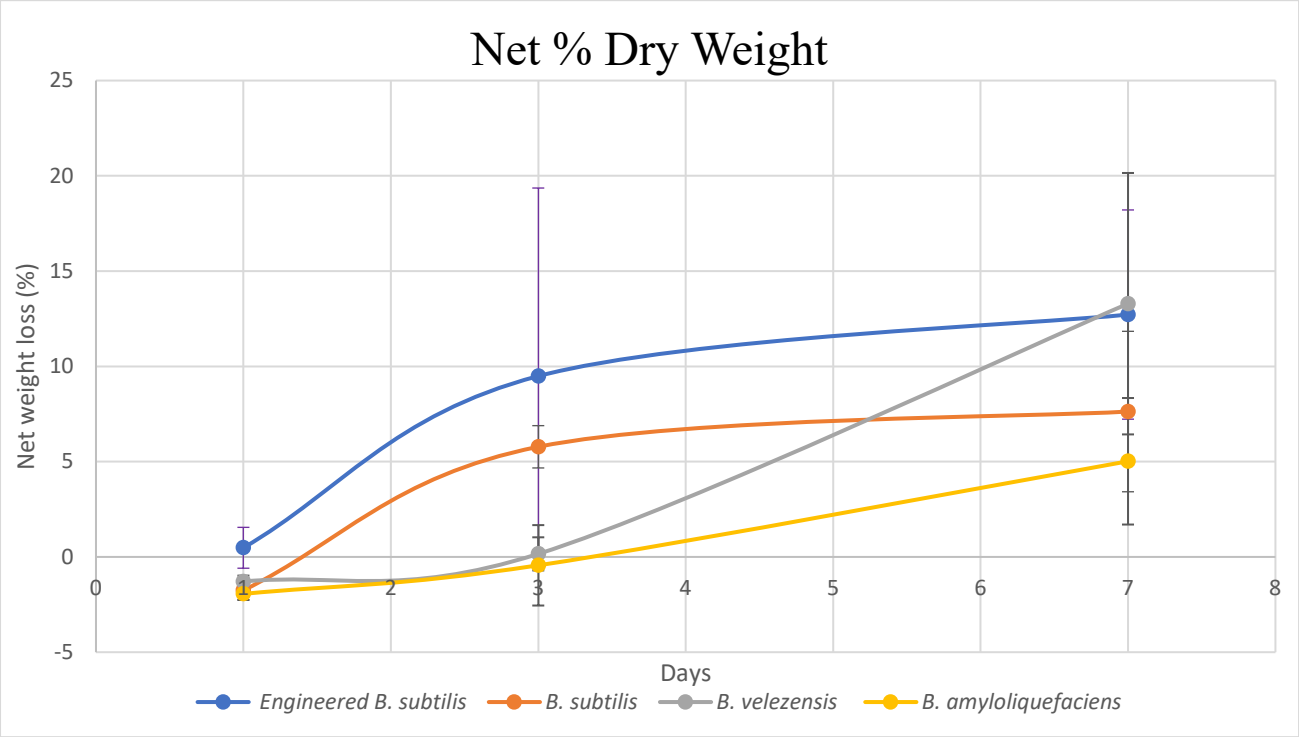


Figure 4.13 Net dry weight loss percentage (%) of paper disks treated with engineered *B. subtilis*, wild-type *B. subtilis, B. velezensis*, and *B. amyloliquefaciens* measured at 1, 3, and 7 days. Values represent the meaning of three biological replicates (n=3).

At 24 h, all wild-type strains (*B. subtilis* , *B. velezensis*, and *B. amyloliquefaciens*) showed negative net weight loss values ranging from -1,2% to -1,9%. This initial weight gain reflects early bacterial attachment and extracellular polymeric substance (EPS) deposition, which could interfere with the paper weight misuration. In contrast, the engineered *B. subtilis* strain showed a positive net weight loss (+0.5%) within the first 24 h, indicating that hyper-secreted endoglucanases immediately surpassed the mass contribution of adhering biomass.

By day 3, a rapid degradation kinetics was evident for the engineered *B. subtilis*, leading to a net weight loss of 9.5%, which strongly correlates with the fiber disintegration observed in SEM micrographs (Fig. 4.9). Conversely, the weight of paper treated by *B. velezensis* (+0.2%) and *B. amyloliquefaciens* (-0.4%) remained near baseline due to persistent biofilm accumulation and endospore aggregation

By day 7, the weight loss caused by the engineered *B. subtilis* approached a plateau at 12,7%, consistent with substrate depletion and late-stage cell autolysis. Interestingly, *B. velezensis* exhibited a marked late-stage surge between days 3 and 7, reaching 13,3% net weight loss.

Overall, these quantitative results confirm that while wild-type strains exhibit delayed paper degradation, the engineered *B. subtilis* drives earlier depolymerization of the cellulosic matrix.

CONCLUSION

The extensive applicability of *Bacillus* species combined with their cellulase production allow for the development of bioactive paper.

To develop this innovative product both in silico and in vitro studies were conducted. Indeed, this thesis tries to cover all the aspects of bioproduct development. Thanks to the bioinformatics analysis it was possible to not only predict the presence of cellulase genes, but also the safety of these species. This analysis showed how species belonging to *subtilis* (*sensu stricto*) show very low, in case of engineered *B. subtilis*, or no (wild-type), antibiotic resistance, thus proving the complete biosafety profile in the usage of bioactive paper containing them.

Another key strength of this thesis is certainly the possibility of testing the strains directly on their actual substrate, the cellulose matrix, rather than on artificial construct, being in this matter able to provide data for practical application.

The experimentations were conducted not only with basic laboratory techniques, but also with novel instruments like flow cytometry and Scanning Electron Microscopy, that corroborate both the bacterial growth and the interaction of bacteria with the paper substrate.

The results clearly showed the high cellulolytic activity of all of the four strains taken into consideration, especially the engineered one which was able to hyperproduce and degrade paper in less time than the other ones, without showing any impact of the genetic modification on growth, as the preliminary studies on bacteria growth demonstrated.

The natural next step could be implementing the same non-GMO technology of *B. subtilis* engineering to *B. velezensis* and *B. amyloliquefaciens*, to improve their cellulase production, without changing their features. In this way it could be possible to maximize the original product performance while fully bypassing the stringent regulatory hurdles associated with GMOs.

Over all, this study represents an example of how this vast genus can represent an important solution for pollution related to cellulose, a bioremediation agent against sewer pipe clogging. However, this is only the beginning: being the paper one of the most used material in different fields (such as tissue products, graphics, packaging and cellulosic textiles) the same *Bacillus* strains can be exploited to improve their degradability, reducing their environmental impact.

REFERENCES

1 Bibliography

Abd Elhameed E, Sayed ARM, Radwan TEE, Hassan G. Biochemical and Molecular Characterization of Five *Bacillus* Isolates Displaying Remarkable Carboxymethyl Cellulase Activities. Curr Microbiol. 2020; 77:3076-3084.

Acho-Vasquez HJ, Henaut-Jacobs S, Venancio TM. Integrative phylogenomic and pangenome landscape of *Bacillus*: insights from 10,000 genomes into taxonomy, functional potential, and biotechnological applications. World J Microbiol Biotechnol. 2025; 42.

Ahmed AS, Bahreini G, Ho D, Sridhar G, Gupta M, Wessels C, Marcelis P, Elbeshbishy E, Rosso D, Santoro D, Nakhla G. Fate of cellulose in primary and secondary treatment at municipal water resource recovery facilities. Water Environ Res. 2019; 91:1479-1489.

Alcaraz LD, Moreno-Hagelsieb G, Eguiarte LE, Souza V, Herrera-Estrella L, Olmedo G. Understanding the evolutionary relationships and major traits of *Bacillus* through comparative genomics. BMC Genomics. 2010; 11:332.

Ayilara MS, Babalola OO. Bioremediation of environmental wastes: the role of microorganisms. Front Agron. 2023.

Balla A, Silini A, Cherif-Silini H, Bouket AC, Boudechicha A, Luptakova L, Alenezi FN, Belbahri L. Screening of Cellulolytic Bacteria from Various Ecosystems and Their Cellulases Production under Multi-Stress Conditions. Catalysts. 2022; 12:769.

Blanco Crivelli X, Cundon C, Bonino MP, Sanin MS, Bentancor A. The Complex and Changing Genus *Bacillus*: A Diverse Bacterial Powerhouse for Many Applications. *Bacteria*. 2024; 3:256-270.

Brutscher LM, Borgmeier C, Garvey S, Spears J. Preclinical Safety Assessment of *Bacillus subtilis* BS50 for Probiotic and Food Applications. *Microorganisms*. 2022; 10:1118.

Chokshi S, Parmar V, Gohil P, Chaudhary V. Chemical Composition and Mechanical Properties of Natural Fibers. *J Nat Fibers*. 2022; 19:3942-3953.

Dobrzyński J, Wróbel B, Górska E. Taxonomy, Ecology, and Cellulolytic Properties of the Genus *Bacillus* and Related Genera. *Agriculture*. 2023; 13:1700.

Elmas G, Bekiroglu S. Effect of toilet tissue Paper on residential sewerage-line clogging. *BioResources*. 2019; 14:7068-7079.

Elmas G, Karabulut B, Bekiroglu S, Atik C, Sönmez S. Disintegration of toilet papers used in shopping malls. *Nord Pulp Paper Res J*. 2023; 38:321-332.

Eren B, Karadagli F. Physical Disintegration of Toilet Papers in Wastewater Systems: Experimental Analysis and Mathematical Modeling. *Environ Sci Technol*. 2012; 46:2870-2876.

Erkihun M, Asmare Z, Endalamew K, Getie B, Kiros T, Berhan A. Medical Scope of Biofilm and Quorum Sensing during Biofilm Formation: Systematic Review. *Bacteria*. 2024; 3:104-123.

Fan B, Blom J, Klenk HP, Borriss R. *Bacillus amyloliquefaciens*, *Bacillus velezensis*, and *Bacillus siamensis* Form an "Operational Group *B. amyloliquefaciens*" within the *B. subtilis* Species Complex. *Front Microbiol*. 2017; 8:22.

Fatani S, Saito Y, Alarawi M, Gojobori T, Mineta K. Genome sequencing and identification of cellulase genes in *Bacillus paralicheniformis* strains from the Red Sea. *BMC Microbiol*. 2021; 21:254.

Gomez del Pulgar EM, Saadeddin A. The cellulolytic system of *Thermobifida fusca*. *Crit Rev Microbiol*. 2014; 40:338-347.

Gupta PK, Raghunath SS, Prasanna DV, Venkat P, Shree V, Chithananthan C, Choudhary S, Surender K, Geetha K. 2019. An Update on Overview of Cellulose, Its Structure and Applications. In: *Cellulose* (Rodriguez A, editor). London: IntechOpen, p. 1–22.

Etesami H, Jeong BR, Glick BR. Biocontrol of plant diseases by *Bacillus* spp. *Physiol Mol Plant Pathol*. 2023; 126:102042.

Harwood CR, editor. 1989. *Bacillus*. Berlin: Springer Science & Business Media.

Herrmann LW, Letti LAJ, Penha RO, Soccol VT, Rodrigues C, Soccol CR. *Bacillus* genus industrial applications and innovation: First steps towards a circular bioeconomy. *Biotechnol Adv*. 2024; 70:108280.

Kour D, Kaur T, Devi R, Yadav A, Singh M, Joshi D, Singh J, Suyal DC, Kumar A, Rajput VD, Yadav AN, Singh K, Singh J, Sayyed RZ, Arora NK, Saxena AK. Beneficial microbiomes for bioremediation of diverse contaminated environments for environmental sustainability: present status and future challenges. *Environ Sci Pollut Res Int*. 2021; 28:24917-24939.

Koutsoumanis K, Allende A, Álvarez-Ordóñez A, Bolton D, Bover-Cid S, Chemaly M, De Cesare A, Hilbert F, Lindqvist R, Nauta M, Nonno R, Peixe L, Ru G, Simmons MM, Skandamis P, Suffredini E, Cocconcelli P, Evaristo Suarez J, Fernandez EN, Herman L. Statement on how to interpret the QPS qualification on 'acquired antimicrobial resistance genes'. *EFSA J*. 2023; 21:e08323.

Krithika V, Geetha K. 2019. An Update on Overview of Cellulose, Its Structure and Applications. In: *Cellulose*(Rodriguez A, editor). London: IntechOpen, p. 1–18.

Liu G, Gong H, Tang H, Meng Z, Wang Z, Cui W, Zhang K, Chen YL, Yang Y. Enhanced lignocellulose degradation in *Bacillus subtilis* RLI2019 through CRISPR/Cas9-mediated chromosomal integration of ternary cellulase genes. *Int J Biol Macromol*. 2025; 306(Pt 3):141727.

Liu L, Huang WC, Liu Y, Li M. Diversity of cellulolytic microorganisms and microbial cellulases. *Int Biodeterior Biodegradation*. 2021; 163:105277.

Lugani Y, Sooch BS. In silico Characterization of Cellulases from Genus *Bacillus*. *Int J Curr Res Rev*. 2017; 9:36-42.

Maalouf A, Mavropoulos A. Re-assessing global municipal solid waste generation. *Waste Manag Res*. 2023; 41:936-947.

Snyder L, Champness W, Henkin TM, Peters JE. 2020. *Molecular Genetics of Bacteria*. 5th ed. Washington (DC): ASM Press.

Dvořák P, Nikel PI, Damborský J, de Lorenzo V. Bioremediation 3.0: Engineering pollutant-removing bacteria in the times of systemic biology. *Biotechnol Adv*. 2017; 35:845-866.

Matilda MI, Samuel HS. Bioremediation of oil spill: concept, methods and applications. *Discov Chem*. 2024; 1:42.

Mohanan N, Montazer Z, Sharma PK, Levin DB. Microbial and Enzymatic Degradation of Synthetic Plastics. *Front Microbiol*. 2020; 11:580709.

Ngalimat MS, Yahaya RSR, Baharudin MMA, Yaminudin SM, Karim M, Ahmad SA, Sabri S. A Review on the Biotechnological Applications of the Operational Group *Bacillus amyloliquefaciens*. *Microorganisms*. 2021; 9:614.

Palmieri S, Cipolletta G, Pastore C, Giosuè C, Akyol Ç, Eusebi AL, Frison N, Tittarelli F, Fatone F. Pilot scale cellulose recovery from sewage sludge and reuse in building and construction material. *Waste Manag*. 2019; 100:208-218.

Pandolfo E, Barra Caracciolo A, Rolando L. Recent Advances in Bacterial Degradation of Hydrocarbons. *Water*. 2023; 15:375.

Parra-Cota FI, Bruno I, García-Montelongo M, González Villarreal S, Delgado M, Córdova-Albores LC, Escalante-Beltrán A, de los Santos-Villalobos S. The genus *Bacillus* as biological control agent against pests and pathogens for sustainable agriculture. *Rev Mex Fitopatol*. 2024; 42:39.

Rabbee MF, Ali MS, Choi J, Hwang BS, Jeong SC, Baek KH. *Bacillus velezensis*: A Valuable Member of Bioactive Molecules within Plant Microbiomes. *Molecules*. 2019; 24:1046.

Raymond RL, Jamison VW, Hudson JO. 1975. *Final Report on Beneficial Stimulation of Bacterial Activity in Ground Waters Containing Petroleum Products*. Marcus Hook (PA): Sun Ventures, Incorporated.

Sahreen S, Mukhtar H, Imre K, Morar A, Herman V, Sharif S. Exploring the Function of Quorum Sensing Regulated Biofilms in Biological Wastewater Treatment: A Review. *Int J Mol Sci*. 2022; 23:6220.

Siddiqi MM, Naseer MN, Wahab Y, Hamizi N, Badruddin I, Abul Hasan M, Chowdhury Z, Akbarzadeh Pivehzhani O, Johan M, Kamangar S. Exploring E-Waste Resources Recovery in Household Solid Waste Recycling. *Processes*. 2020; 8:1047.

Singh S. The Role of Environmental Microbiota in Bioremediation: Harnessing Bacteria for Pollutant Degradation. *Clin Med Health Res J*. 2025.

Stülke J, Grüppen A, Bramkamp M, Pelzer S. *Bacillus subtilis*, a Swiss Army Knife in Science and Biotechnology. *J Bacteriol*. 2023; 205:e0010223.

Vincze S, Dahouk AS, Dieckmann R. Microbiological Safety of Non-Food Products: What Can We Learn from the RAPEX Database?. *Int J Environ Res Public Health*. 2019; 16:1599.

Wang X, Liu G, Sun W, Cao Z, Liu H, Xiong Y, Li B, Sun X, Li Y, Xu R, Huang D, Gao P. Removal of toilet paper fibers from residential wastewater: a life cycle assessment. *Environ Sci Pollut Res Int*. 2023; 30:84254-84266.

Wang Y, Deng H, Li ZC, Tan YF, Han YP, Wang X, Du Z, Liu Y, Yang RF, Bai Y, Bi Y, Zhi FC. Safety Evaluation of a Novel Strain of *Bacteroides fragilis*. *Front Microbiol*. 2017; 8:435.

Wegmann U, Carvalho A, Stocks M, Carding S. Use of genetically modified bacteria for drug delivery in humans: Revisiting the safety aspect. *Sci Rep*. 2017; 7:2294.

World Health Organization. 2022. World Health Day 2022: Our planet, our health. Disponibile su: https://www.who.int/campaigns/world-health-day/2022

Yao Y, Wang L, Zhai H, et al. *Bacillus velezensis* A-27 as a potential biocontrol agent against *Meloidogyne incognita*and effects on rhizosphere communities of celery in field. *Sci Rep*. 2025; 15:1057.

Zeng Q, Zhao Y, Zhuang L, Jiang W, Wang L, Zhang J, Wang L, Guo H, Li Y, Wang Z, Li Y, Wang Q.Comparative genomics of *Bacillus velezensis* and *Bacillus subtilis* reveals distinction and evolution of lipopeptide antimicrobial gene clusters. *BMC Genomics*. 2025; 26:1071.

2 Sitography

DTU, center for genomic epidemiology, https://genepi.food.dtu.dk/services/ResFinder

Floreada.io, https://floreada.io

UniProt, https://www.uniprot.org

United Nations (2015). The 17 goals, https://sdgs.un.org/goals

World Health Organization. 2022. World Health Day 2022: Our planet, our health. https://www.who.int/campaigns/world-health-day/2022

3 Supporting materials

I TBLAST genomic analysis raw data

The following tables are the outputs of TBLAST between engineered *B. subtilis* genome and cellulase amino acids sequence:

sp|P10475|GUN2_BACSU	CP007800.1	100.000	499	100	0.0
sp|P10475|GUN2_BACSU	CP007800.1	48.000	25	100	3.1
sp|P10475|GUN2_BACSU	CP007800.1	20.755	53	100	6.8

Table I Raw output of TBLAST search between the engineered *B. subtilis* genome and the amino acid sequence of endoglucanase P10475. Columns from left to right represent: Query ID, Subject Accession, Percentage Identity (%), Alignment Length, Bit Score, and E-value.

sp|O05508|GMUD_BACSU	CP007800.1	99.785	465	100	0.0
sp|O05508|GMUD_BACSU	CP007800.1	36.175	481	100	6.29e-88
sp|O05508|GMUD_BACSU	CP007800.1	33.333	483	100	1.72e-66
sp|O05508|GMUD_BACSU	CP007800.1	31.340	485	100	9.38e-59

Table II Raw output of TBLAST search between the engineered *B. subtilis* genome and the amino acid sequence of ß-glucosidase O05508. Columns from left to right represent: Query ID, Subject Accession, Percentage Identity (%), Alignment Length, Bit Score, and E-value.

The following tables are the outputs of TBLAST between *B. subtilis* genome and cellulase amino acids sequence:

sp|P10475|GUN2_BACSU	Bacillus	97.395	499	0.0	914
sp|P10475|GUN2_BACSU	Bacillus	48.000	25	3.7	27.3
sp|P10475|GUN2_BACSU	Bacillus	20.755	53	6.8	26.6
sp|P10475|GUN2_BACSU	Bacillus	36.667	30	7.8	26.2

Table III Raw output of TBLAST search between *B. subtilis* genome and the amino acid sequence of endoglucanase P10475. Columns from left to right represent: Query ID, Subject Accession, Percentage Identity (%), Alignment Length, E-value and Bit Score.

sp|O05508|GMUD_BACSU	Bacillus	98.710	465	100	0.0
sp|O05508|GMUD_BACSU	Bacillus	35.551	481	100	1.24e-85
sp|O05508|GMUD_BACSU	Bacillus	33.612	479	100	2.92e-66
sp|O05508|GMUD_BACSU	Bacillus	31.340	485	100	2.62e-58

Table IV Raw output of TBLAST search between *B. subtilis* genome and the amino acid sequence of ß-glucosidase O05508. Columns from left to right represent: Columns from left to right represent: Query ID, Subject Accession, Percentage Identity (%), Alignment Length, Bit Score, and E-value.

The following tables are the outputs of TBLAST between *B. velezensis* genome and cellulase amino acids sequence:

sp|P10475|GUN2_BACSU	B-velezensis	93.174	498	99	0.0
sp|P10475|GUN2_BACSU	B-velezensis	29.825	57	99	4.0
sp|P10475|GUN2_BACSU	B-velezensis	24.211	95	99	5.3
sp|P10475|GUN2_BACSU	B-velezensis	50.000	30	99	5.8

Table V Raw output of TBLAST search between *B. velezensis* genome and the amino acid sequence of endoglucanase P10475. Columns from left to right represent: Query ID, Subject Accession, Percentage Identity (%), Alignment Length, Bit Score, and E-value.

sp|O05508|GMUD_BACSU	B-velezensis	81.739	460	100	0.0
sp|O05508|GMUD_BACSU	B-velezensis	34.255	470	100	5.94e-78
sp|O05508|GMUD_BACSU	B-velezensis	33.402	485	100	5.29e-64
sp|O05508|GMUD_BACSU	B-velezensis	45.455	33	100	0.026
sp|O05508|GMUD_BACSU	B-velezensis	44.444	27	100	0.092
sp|O05508|GMUD_BACSU	B-velezensis	30.000	50	100	1.8
sp|O05508|GMUD_BACSU	B-velezensis	23.188	138	100	2.9
sp|O05508|GMUD_BACSU	B-velezensis	27.083	48	100	3.7
sp|O05508|GMUD_BACSU	B-velezensis	37.500	32	100	4.6
sp|O05508|GMUD_BACSU	B-velezensis	32.653	49	100	6.6

Table VI Raw output of TBLAST search between *B. velezensis* genome and the amino acid sequence of ß-glucosidase O05508. Columns from left to right represent: Query ID, Subject Accession, Percentage Identity (%), Alignment Length, Bit Score, and E-value.

The following tables are the outputs of TBLAST between *B. amyloliquefaciens* genome and cellulase amino acids sequence:

sp|P10475|GUN2_BACSU	B-amyloliquefaciens	93.387	499	100	0.0
sp|P10475|GUN2_BACSU	B-amyloliquefaciens	21.875	128	100	3.4
sp|P10475|GUN2_BACSU	B-amyloliquefaciens	50.000	30	100	6.1
sp|P10475|GUN2_BACSU	B-amyloliquefaciens	45.161	31	100	6.2

Table VII Raw output of TBLAST search between *B. amyloliquefaciens* genome and the amino acid sequence of endoglucanase P10475. Columns from left to right represent: Query ID, Subject Accession, Percentage Identity (%), Alignment Length, Bit Score, and E-value.

tr|A8FDC4|A8FDC4_BACP2	B-amyloliquefaciens	57.143	21	20	2.9
tr|A8FDC4|A8FDC4_BACP2	B-amyloliquefaciens	35.294	34	20	3.2
tr|A8FDC4|A8FDC4_BACP2	B-amyloliquefaciens	30.645	62	20	6.1
tr|A8FDC4|A8FDC4_BACP2	B-amyloliquefaciens	37.500	32	20	8.5

Table IX Raw output of TBLAST search between *B. amyloliquefaciens* genome and the amino acid sequence of exoglucanase A8FDC4. Columns from left to right represent: Query ID, Subject Accession, Percentage Identity (%), Alignment Length, Bit Score, and E-value

sp|O05508|GMUD_BACSU	B-amyloliquefaciens	82.174	460	100	0.0
sp|O05508|GMUD_BACSU	B-amyloliquefaciens	34.255	470	100	3.15e-78
sp|O05508|GMUD_BACSU	B-amyloliquefaciens	33.608	485	100	1.22e-63
sp|O05508|GMUD_BACSU	B-amyloliquefaciens	45.312	64	100	1.36e-08
sp|O05508|GMUD_BACSU	B-amyloliquefaciens	47.368	38	100	9.03e-05
sp|O05508|GMUD_BACSU	B-amyloliquefaciens	30.000	50	100	1.8
sp|O05508|GMUD_BACSU	B-amyloliquefaciens	24.359	78	100	1.9
sp|O05508|GMUD_BACSU	B-amyloliquefaciens	27.083	48	100	3.7
sp|O05508|GMUD_BACSU	B-amyloliquefaciens	32.653	49	100	6.3
sp|O05508|GMUD_BACSU	B-amyloliquefaciens	34.375	32	100	7.9

Table IX Raw output of TBLAST search between *B. amyloliquefaciens* genome and the amino acid sequence of ß-glucosidase O05508. Columns from left to right represent: Query ID, Subject Accession, Percentage Identity (%), Alignment Length, Bit Score, and E-value

Note: the Exoglucanase BLAST search outputs of some strains are not included in the Supporting materials as no sequence alignment or overlap was detected across any of the target *Bacillus* genomes, producing empty result files.

II Antimicrobial resistance screening raw data

The following raw output reports the in silico antimicrobial resistance phenotype predictions generated using ResFinder for the engineered *Bacillus subtilis* genome assembly:

```
# ResFinder phenotype results.
# Sample: GCA_000699465.1_ASM69946v1_genomic.fna
#
# The phenotype 'No resistance' should be interpreted with
# caution, as it only means that nothing in the used
# database indicate resistance, but resistance could exist
# from 'unknown' or not yet implemented sources.
#
# The 'Match' column stores one of the integers 0, 1, 2, 3.
#      0: No match found
#      1: Match < 100% ID AND match length < ref length
#      2: Match = 100% ID AND match length < ref length
#      3: Match = 100% ID AND match length = ref length
# If several hits causing the same resistance are found,
# the highest number will be stored in the 'Match' column.

# Antimicrobial  Class WGS-predicted phenotype     Match Genetic background
gentamicin aminoglycoside   No resistance    0
tobramycin aminoglycoside   No resistance    0
streptomycin     aminoglycoside   Resistant  3     aadK (aadK_M26879)
amikacin   aminoglycoside   No resistance    0
isepamicin aminoglycoside   No resistance    0
dibekacin  aminoglycoside   No resistance    0
kanamycin  aminoglycoside   No resistance    0
neomycin   aminoglycoside   No resistance    0
lividomycinaminoglycoside   No resistance    0
paromomycinaminoglycoside   No resistance    0
ribostamycin     aminoglycoside   No resistance    0
unknown aminoglycoside aminoglycoside   No resistance    0
butiromycinaminoglycoside   No resistance    0
butirosin  aminoglycoside   No resistance    0
hygromycin aminoglycoside   No resistance    0
netilmicin aminoglycoside   No resistance    0
apramycin  aminoglycoside   No resistance    0
sisomicin  aminoglycoside   No resistance    0
arbekacin  aminoglycoside   No resistance    0
kasugamycinaminoglycoside   No resistance    0
astromicin aminoglycoside   No resistance    0
fortimicin aminoglycoside   No resistance    0
spectinomycin    aminocyclitol    No resistance    0
fluoroquinolone  quinolone  No resistance    0
ciprofloxacin    quinolone  No resistance    0
unknown quinolone     quinolone  No resistance    0
nalidixic acid   quinolone  No resistance    0
amoxicillinbeta-lactamNo resistance    0
amoxicillin+clavulanic acid beta-lactamNo resistance    0
ampicillin beta-lactamNo resistance    0
ampicillin+clavulanic acid  beta-lactamNo resistance    0
cefepime   beta-lactamNo resistance    0
cefixime   beta-lactamNo resistance    0
```

cefotaxime beta-lactamNo resistance 0
cefoxitin beta-lactamNo resistance 0
ceftazidimebeta-lactamNo resistance 0
ertapenem beta-lactamNo resistance 0
imipenem beta-lactamNo resistance 0
meropenem beta-lactamNo resistance 0
piperacillin beta-lactamNo resistance 0
piperacillin+tazobactam beta-lactamNo resistance 0
unknown beta-lactam beta-lactamNo resistance 0
aztreonam beta-lactamNo resistance 0
cefotaxime+clavulanic acid beta-lactamNo resistance 0
temocillin beta-lactamNo resistance 0
ticarcillinbeta-lactamNo resistance 0
ceftazidime+avibactam beta-lactamNo resistance 0
penicillin beta-lactamNo resistance 0
ceftriaxonebeta-lactamNo resistance 0
ticarcillin+clavulanic acid beta-lactamNo resistance 0
cephalothinbeta-lactamNo resistance 0
piperacillin+clavulanic acidbeta-lactamNo resistance 0
ceftiofur under_development No resistance 0
sulfamethoxazole folate pathway antagonist No resistance 0
trimethoprim folate pathway antagonist No resistance 0
fosfomycin fosfomycin No resistance 0
vancomycin glycopeptide No resistance 0
teicoplaninglycopeptide No resistance 0
bleomycin glycopeptide No resistance 0
lincomycin lincosamideNo resistance 0
clindamycinlincosamideNo resistance 0
dalfopristin streptogramin a No resistance 0
pristinamycin iia streptogramin a No resistance 0
virginiamycin m streptogramin a No resistance 0
quinupristin+dalfopristin streptogramin a No resistance 0
tiamulin pleuromutilin No resistance 0
carbomycin macrolide No resistance 0
erythromycin macrolide No resistance 0
azithromycin macrolide No resistance 0
oleandomycin macrolide No resistance 0
spiramycin macrolide Resistant 3 mph(K) (mph(K)_NC_000964)
tylosin macrolide No resistance 0
telithromycin macrolide Resistant 3 mph(K) (mph(K)_NC_000964)
tetracycline tetracycline Resistant 3 tet(L) (tet(L)_X08034)
doxycyclinetetracycline Resistant 3 tet(L) (tet(L)_X08034)
minocyclinetetracycline No resistance 0
tigecyclinetetracycline No resistance 0
quinupristin streptogramin b No resistance 0
pristinamycin ia streptogramin b No resistance 0
virginiamycin s streptogramin b No resistance 0
linezolid oxazolidinone No resistance 0
chloramphenicol amphenicol No resistance 0
florfenicolamphenicol No resistance 0
colistin polymyxin No resistance 0
fusidic acid steroid antibacterial No resistance 0
mupirocin pseudomonic acid No resistance 0
rifampicin rifamycin No resistance 0
metronidazole nitroimidazole No resistance 0
narasin ionophores No resistance 0
salinomycinionophores No resistance 0
maduramicinionophores No resistance 0

Below are the raw ResFinder screening results predicting the *in silico* antimicrobial resistance profile of *Bacillus subtilis* genome assembly:

```
# Resistence Finder: phenotype results.
# Sample: B-subtilisCA
#
# The phenotype 'No resistance' should be interpreted with
# caution, as it only means that nothing in the used
# database indicate resistance, but resistance could exist
# from 'unknown' or not yet implemented sources.
#
# The 'Match' column stores one of the integers 0, 1, 2, 3.
#      0: No match found
#      1: Match < 100% ID AND match length < ref length
#      2: Match = 100% ID AND match length < ref length
#      3: Match = 100% ID AND match length = ref length
# If several hits causing the same resistance are found,
# the highest number will be stored in the 'Match' column.

# Antimicrobial  Class WGS-predicted phenotype     Match Genetic background
gentamicin aminoglycoside   No resistance    0
tobramycin aminoglycoside   No resistance    0
streptomycin     aminoglycoside   No resistance    0
amikacin   aminoglycoside   No resistance    0
isepamicin aminoglycoside   No resistance    0
dibekacin  aminoglycoside   No resistance    0
kanamycin  aminoglycoside   No resistance    0
neomycin   aminoglycoside   No resistance    0
lividomycinaminoglycoside   No resistance    0
paromomycinaminoglycoside   No resistance    0
ribostamycin     aminoglycoside   No resistance    0
butiromycinaminoglycoside   No resistance    0
butirosin  aminoglycoside   No resistance    0
hygromycin aminoglycoside   No resistance    0
netilmicin aminoglycoside   No resistance    0
apramycin  aminoglycoside   No resistance    0
sisomicin  aminoglycoside   No resistance    0
arbekacin  aminoglycoside   No resistance    0
kasugamycinaminoglycoside   No resistance    0
astromicin aminoglycoside   No resistance    0
fortimicin aminoglycoside   No resistance    0
spectinomycin    aminocyclitol    No resistance    0
fluoroquinolone  quinolone  No resistance    0
ciprofloxacin    quinolone  No resistance    0
nalidixic acid   quinolone  No resistance    0
amoxicillinbeta-lactamNo resistance    0
amoxicillin+clavulanic acid beta-lactamNo resistance    0
ampicillin beta-lactamNo resistance    0
ampicillin+clavulanic acid  beta-lactamNo resistance    0
cefepime   beta-lactamNo resistance    0
cefixime   beta-lactamNo resistance    0
cefotaxime beta-lactamNo resistance    0
cefoxitin  beta-lactamNo resistance    0
ceftazidimebeta-lactamNo resistance    0
ertapenem  beta-lactamNo resistance    0
```

imipenem beta-lactam No resistance 0
meropenem beta-lactam No resistance 0
piperacillin beta-lactam No resistance 0
piperacillin+tazobactam beta-lactam No resistance 0
aztreonam beta-lactam No resistance 0
cefotaxime+clavulanic acid beta-lactam No resistance 0
temocillin beta-lactam No resistance 0
ticarcillin beta-lactam No resistance 0
ceftazidime+avibactam beta-lactam No resistance 0
penicillin beta-lactam No resistance 0
ceftriaxone beta-lactam No resistance 0
ticarcillin+clavulanic acid beta-lactam No resistance 0
cephalothin beta-lactam No resistance 0
cephalotin beta-lactam No resistance 0
piperacillin+clavulanic acid beta-lactam No resistance 0
ceftiofur under_development No resistance 0
sulfamethoxazole folate pathway antagonist No resistance 0
trimethoprim folate pathway antagonist No resistance 0
fosfomycin fosfomycin No resistance 0
vancomycin glycopeptide No resistance 0
teicoplanin glycopeptide No resistance 0
bleomycin glycopeptide No resistance 0
lincomycin lincosamide No resistance 0
clindamycin lincosamide No resistance 0
dalfopristin streptogramin a No resistance 0
pristinamycin iia streptogramin a No resistance 0
virginiamycin m streptogramin a No resistance 0
quinupristin+dalfopristin streptogramin a No resistance 0
tiamulin pleuromutilin No resistance 0
carbomycin macrolide No resistance 0
erythromycin macrolide No resistance 0
azithromycin macrolide No resistance 0
oleandomycin macrolide No resistance 0
spiramycin macrolide No resistance 0
tylosin macrolide No resistance 0
telithromycin macrolide No resistance 0
tetracycline tetracycline No resistance 0
doxycycline tetracycline No resistance 0
minocycline tetracycline No resistance 0
tigecycline tetracycline No resistance 0
quinupristin streptogramin b No resistance 0
pristinamycin ia streptogramin b No resistance 0
virginiamycin s streptogramin b No resistance 0
linezolid oxazolidinone No resistance 0
chloramphenicol amphenicol No resistance 0
florfenicol amphenicol No resistance 0
colistin polymyxin No resistance 0
fusidic acid steroid antibacterial No resistance 0
mupirocin pseudomonic acid No resistance 0
rifampicin rifamycin No resistance 0
metronidazole nitroimidazole No resistance 0
narasin ionophores No resistance 0
salinomycin ionophores No resistance 0
maduramicin ionophores No resistance 0

The raw data presented below detail the *in silico* antimicrobial resistance predictions obtained via ResFinder analysis for *Bacillus velezensis* genome assembly:

```
# ResFinder phenotype results.
# Sample: Bacillus_velezensis.fa
#
# The phenotype 'No resistance' should be interpreted with
# caution, as it only means that nothing in the used
# database indicate resistance, but resistance could exist
# from 'unknown' or not yet implemented sources.
#
# The 'Match' column stores one of the integers 0, 1, 2, 3.
#      0: No match found
#      1: Match < 100% ID AND match length < ref length
#      2: Match = 100% ID AND match length < ref length
#      3: Match = 100% ID AND match length = ref length
# If several hits causing the same resistance are found,
# the highest number will be stored in the 'Match' column.

# Antimicrobial  Class WGS-predicted phenotype     Match Genetic background
gentamicin aminoglycoside   No resistance    0
tobramycin aminoglycoside   No resistance    0
streptomycin     aminoglycoside   No resistance    0
amikacin   aminoglycoside   No resistance    0
isepamicin aminoglycoside   No resistance    0
dibekacin  aminoglycoside   No resistance    0
kanamycin  aminoglycoside   No resistance    0
neomycin   aminoglycoside   No resistance    0
lividomycinaminoglycoside   No resistance    0
paromomycinaminoglycoside   No resistance    0
ribostamycin     aminoglycoside   No resistance    0
unknown aminoglycoside aminoglycoside   No resistance    0
butiromycinaminoglycoside   No resistance    0
butirosin  aminoglycoside   No resistance    0
hygromycin aminoglycoside   No resistance    0
netilmicin aminoglycoside   No resistance    0
apramycin  aminoglycoside   No resistance    0
sisomicin  aminoglycoside   No resistance    0
arbekacin  aminoglycoside   No resistance    0
kasugamycinaminoglycoside   No resistance    0
astromicin aminoglycoside   No resistance    0
fortimicin aminoglycoside   No resistance    0
spectinomycin    aminocyclitol    No resistance    0
fluoroquinolone  quinolone  No resistance    0
ciprofloxacin    quinolone  No resistance    0
unknown quinolone     quinolone  No resistance    0
nalidixic acid   quinolone  No resistance    0
amoxicillinbeta-lactamNo resistance    0
amoxicillin+clavulanic acid beta-lactamNo resistance    0
ampicillin beta-lactamNo resistance    0
ampicillin+clavulanic acid  beta-lactamNo resistance    0
cefepime   beta-lactamNo resistance    0
cefixime   beta-lactamNo resistance    0
cefotaxime beta-lactamNo resistance    0
cefoxitin  beta-lactamNo resistance    0
ceftazidimebeta-lactamNo resistance    0
```

```
ertapenem  beta-lactamNo resistance    0
imipenem   beta-lactamNo resistance    0
meropenem  beta-lactamNo resistance    0
piperacillin     beta-lactamNo resistance    0
piperacillin+tazobactam     beta-lactamNo resistance    0
unknown beta-lactam    beta-lactamNo resistance    0
aztreonam  beta-lactamNo resistance    0
cefotaxime+clavulanic acid  beta-lactamNo resistance    0
temocillin beta-lactamNo resistance    0
ticarcillinbeta-lactamNo resistance    0
ceftazidime+avibactam  beta-lactamNo resistance    0
penicillin beta-lactamNo resistance    0
ceftriaxonebeta-lactamNo resistance    0
ticarcillin+clavulanic acid beta-lactamNo resistance    0
cephalothinbeta-lactamNo resistance    0
piperacillin+clavulanic acidbeta-lactamNo resistance    0
ceftiofur  under_development     No resistance    0
sulfamethoxazole folate pathway antagonist   No resistance    0
trimethoprim     folate pathway antagonist   No resistance    0
fosfomycin fosfomycin No resistance    0
vancomycin glycopeptide     No resistance    0
teicoplaninglycopeptide     No resistance    0
bleomycin  glycopeptide     No resistance    0
lincomycin lincosamideNo resistance    0
clindamycinlincosamideNo resistance    0
dalfopristin     streptogramin a  No resistance    0
pristinamycin iia     streptogramin a  No resistance    0
virginiamycin m  streptogramin a  No resistance    0
quinupristin+dalfopristin   streptogramin a  No resistance    0
tiamulin   pleuromutilin    No resistance    0
carbomycin macrolide  No resistance    0
erythromycin     macrolide  No resistance    0
azithromycin     macrolide  No resistance    0
oleandomycin     macrolide  No resistance    0
spiramycin macrolide  No resistance    0
tylosin    macrolide  No resistance    0
telithromycin    macrolide  No resistance    0
tetracycline     tetracycline     No resistance    0
doxycyclinetetracycline     No resistance    0
minocyclinetetracycline     No resistance    0
tigecyclinetetracycline     No resistance    0
quinupristin     streptogramin b  No resistance    0
pristinamycin ia streptogramin b  No resistance    0
virginiamycin s  streptogramin b  No resistance    0
linezolid  oxazolidinone    No resistance    0
chloramphenicol  amphenicol No resistance    0
florfenicolamphenicol No resistance    0
colistin   polymyxin  No resistance    0
fusidic acid     steroid antibacterial  No resistance    0
mupirocin  pseudomonic acid No resistance    0
rifampicin rifamycin  No resistance    0
metronidazole    nitroimidazole   No resistance    0
narasin    ionophores No resistance    0
salinomycinionophores No resistance    0
maduramicinionophores No resistance    0
formaldehyde     aldehyde   No resistance    0
benzylkonium chloride  quaternary ammonium compoundNo resistance    0
ethidium bromide quaternary ammonium compoundNo resistance    0
```

```
chlorhexidine    quaternary ammonium compoundNo resistance    0
cetylpyridinium chloride    quaternary ammonium compoundNo resistance    0

hydrogen peroxide     peroxide   No resistance    0
temperatureheat  No resistance    0
```

The following raw output outlines the *in-silico* AMR phenotype predictions generated by ResFinder for the *Bacillus amyloliquefaciens* genome assembly:

```
# Resistance Finder phenotype results.
# Sample: B-amyloliquefaciens
#
# The phenotype 'No resistance' should be interpreted with
# caution, as it only means that nothing in the used
# database indicate resistance, but resistance could exist
# from 'unknown' or not yet implemented sources.
#
# The 'Match' column stores one of the integers 0, 1, 2, 3.
#      0: No match found
#      1: Match < 100% ID AND match length < ref length
#      2: Match = 100% ID AND match length < ref length
#      3: Match = 100% ID AND match length = ref length
# If several hits causing the same resistance are found,
# the highest number will be stored in the 'Match' column.

# Antimicrobial  Class WGS-predicted phenotype     Match Genetic background
gentamicin aminoglycoside   No resistance    0
tobramycin aminoglycoside   No resistance    0
streptomycin     aminoglycoside   No resistance    0
amikacin   aminoglycoside   No resistance    0
isepamicin aminoglycoside   No resistance    0
dibekacin  aminoglycoside   No resistance    0
kanamycin  aminoglycoside   No resistance    0
neomycin   aminoglycoside   No resistance    0
lividomycinaminoglycoside   No resistance    0
paromomycinaminoglycoside   No resistance    0
ribostamycin     aminoglycoside   No resistance    0
unknown aminoglycoside aminoglycoside   No resistance    0
butiromycinaminoglycoside   No resistance    0
butirosin  aminoglycoside   No resistance    0
hygromycin aminoglycoside   No resistance    0
netilmicin aminoglycoside   No resistance    0
apramycin  aminoglycoside   No resistance    0
sisomicin  aminoglycoside   No resistance    0
arbekacin  aminoglycoside   No resistance    0
kasugamycinaminoglycoside   No resistance    0
astromicin aminoglycoside   No resistance    0
fortimicin aminoglycoside   No resistance    0
spectinomycin    aminocyclitol    No resistance    0
fluoroquinolone  quinolone  No resistance    0
ciprofloxacin    quinolone  No resistance    0
unknown quinolone      quinolone  No resistance    0
nalidixic acid   quinolone  No resistance    0
amoxicillinbeta-lactamNo resistance    0
amoxicillin+clavulanic acid beta-lactamNo resistance    0
```

```
ampicillin beta-lactamNo resistance    0
ampicillin+clavulanic acid  beta-lactamNo resistance    0
cefepime   beta-lactamNo resistance    0
cefixime   beta-lactamNo resistance    0
cefotaxime beta-lactamNo resistance    0
cefoxitin  beta-lactamNo resistance    0
ceftazidimebeta-lactamNo resistance    0
ertapenem  beta-lactamNo resistance    0
imipenem   beta-lactamNo resistance    0
meropenem  beta-lactamNo resistance    0
piperacillin     beta-lactamNo resistance    0
piperacillin+tazobactam     beta-lactamNo resistance    0
unknown beta-lactam    beta-lactamNo resistance    0
aztreonam  beta-lactamNo resistance    0
cefotaxime+clavulanic acid  beta-lactamNo resistance    0
temocillin beta-lactamNo resistance    0
ticarcillinbeta-lactamNo resistance    0
ceftazidime+avibactam  beta-lactamNo resistance    0
penicillin beta-lactamNo resistance    0
ceftriaxonebeta-lactamNo resistance    0
ticarcillin+clavulanic acid beta-lactamNo resistance    0
cephalothinbeta-lactamNo resistance    0
cephalotin beta-lactamNo resistance    0
piperacillin+clavulanic acidbeta-lactamNo resistance    0
ceftiofur  under_development     No resistance    0
sulfamethoxazole folate pathway antagonist   No resistance    0
trimethoprim     folate pathway antagonist   No resistance    0
fosfomycin fosfomycin No resistance    0
vancomycin glycopeptide     No resistance    0
teicoplaninglycopeptide     No resistance    0
bleomycin  glycopeptide     No resistance    0
lincomycin lincosamideNo resistance    0
clindamycinlincosamideNo resistance    0
dalfopristin     streptogramin a  No resistance    0
pristinamycin iia     streptogramin a  No resistance    0
virginiamycin m  streptogramin a  No resistance    0
quinupristin+dalfopristin   streptogramin a  No resistance    0
tiamulin   pleuromutilin    No resistance    0
carbomycin macrolide  No resistance    0
erythromycin     macrolide  No resistance    0
azithromycin     macrolide  No resistance    0
oleandomycin     macrolide  No resistance    0
spiramycin macrolide  No resistance    0
tylosin    macrolide  No resistance    0
telithromycin    macrolide  No resistance    0
tetracycline     tetracycline     No resistance    0
doxycyclinetetracycline     No resistance    0
minocyclinetetracycline     No resistance    0
tigecyclinetetracycline     No resistance    0
quinupristin     streptogramin b  No resistance    0
pristinamycin ia streptogramin b  No resistance    0
virginiamycin s  streptogramin b  No resistance    0
linezolid  oxazolidinone    No resistance    0
chloramphenicol  amphenicol No resistance    0
florfenicolamphenicol No resistance    0
colistin   polymyxin  No resistance    0
fusidic acid     steroid antibacterial  No resistance    0
mupirocin  pseudomonic acid No resistance    0
```

rifampicin	rifamycin	No resistance	0
metronidazole	nitroimidazole	No resistance	0
narasin	ionophores	No resistance	0
salinomycin	ionophores	No resistance	0
maduramicin	ionophores	No resistance	0

Acknowledgment

Note on AI use: This thesis was checked for grammar and language using Gemini. Gemini was used strictly for paraphrasing and refining the writing. All scientific content, analyses and interpretations are entirely my own.